ORACLE 2-D (v2.0): An efficient module to compute the volatility and oxygen content of organic aerosol with a global chemistry – climate model

Alexandra P. Tsimpidi[1], Vlassis A. Karydis[1], Andrea Pozzer[1], Spyros N. Pandis[2,3] and Jos Lelieveld[1,4]

[1] Max Planck Institute for Chemistry, Mainz, Germany

[2] Department of Chemical Engineering, University of Patras, Patras, Greece

[3] Department of Chemical Engineering, Carnegie Mellon University, Pittsburgh, PA, USA

[4] Energy, Environment and Water Research Center, Cyprus Institute, Nicosia, Cyprus

*Corresponding author e-mail: a.tsimpidi@mpic.de

12   **Abstract**

13   A new module, ORACLE 2-D, simulating the organic aerosol formation and evolution in the

14   atmosphere has been developed and evaluated. The module calculates the concentrations of

15   surrogate organic species in two-dimensional space defined by volatility and oxygen-to-carbon

16   ratio. It is implemented into the EMAC global chemistry – climate model, and a comprehensive

17   evaluation of its performance is conducted using an Aerosol Mass Spectrometer (AMS) factor

18   analysis dataset derived from almost all major field campaigns that took place globally during

19   the period 2001-2010. ORACLE 2-D uses a simple photochemical aging scheme that simulates

20   efficiently the net effects of fragmentation and functionalization of the organic compounds. The

21   module predicts not only the mass concentration of organic aerosol (OA) components, but also

22   their oxidation state (in terms of O:C), which allows their classification into primary OA (POA,

23   chemically unprocessed), fresh secondary OA (SOA, low oxygen content) and aged SOA (highly

24   oxygenated). The explicit simulation of chemical OA conversion from freshly emitted

25   compounds to a highly oxygenated state during photochemical aging enables the tracking of

26   hygroscopicity changes of OA that result from these reactions. ORACLE 2-D can thus compute

27   the ability of OA particles to act as cloud condensation nuclei, and serves a tool to quantify the

28   climatic impact of OA.

30   **1. Introduction**

31   Atmospheric aerosols adversely affect human health and play a significant role in climate

32   change on regional and global scales. Depending on their composition, aerosols affect the energy

33   budget of the Earth's atmosphere by scattering and absorbing solar radiation (direct effect) and

34   by influencing the reflective properties of clouds, their lifetime, and precipitation formation

35   (indirect effects). In addition, climate change can play vital and complex role in the formation

36   and removal of atmospheric particles (Trail et al., 2013;Trail et al., 2014) .Organic aerosol (OA)

37   is an important constituent of atmospheric particles contributing 20-90% to the total submicron

38   particulate mass, depending on the region (Zhang et al., 2007).

39   Primary OA has been traditionally treated as non-volatile and inert in global scale chemistry

40   climate models (CCMs). Robinson et al. (2007) demonstrated that OA emissions are semi-

41   volatile and most of the emitted OA moves to the gas phase after emission due to dilution and

42   evaporation. On the other hand, all organic vapors are subject to photochemical reactions with

OH in the gas phase forming organic products with lower volatility that can recondense to the particulate phase as secondary organic aerosol (SOA). To describe the OA pas-aerosol partitioning, Donahue et al. (2006) developed the volatility basis-set (VBS) framework, where OA is assumed to be semi-volatile and photochemically reactive, and is distributed in logarithmically spaced volatility bins. With this innovative approach, the semi-volatile primary emissions, the chemical aging, and the SOA formation were unified within a common framework that is ideally suited for regional and global chemical modeling. Since 2006, many regional (Lane et al., 2008;Murphy and Pandis, 2009;Tsimpidi et al., 2010;Tsimpidi et al., 2011;Ahmadov et al., 2012;Athanasopoulou et al., 2013;Koo et al., 2014;Fountoukis et al., 2014;Ciarelli et al., 2017;Gao et al., 2017) and global (Pye and Seinfeld, 2010;Jathar et al., 2011;Jo et al., 2013;Tsimpidi et al., 2014;Hodzic et al., 2016) modeling studies have used the VBS to account for the semi-volatile nature and chemical aging of organic compounds, demonstrating improvements in reproducing the OA budget and its chemical resolution.

The chemical aging of OA results in significant changes of its physical and chemical properties due to the addition of oxygen atoms from the reaction with OH. This increase in OA oxygen content is important for its impact on climate through changes in cloud condensation nuclei (CCN) and ice nuclei (IN) activity. In fact, the oxygen content, expressed by the ratio of oxygen to carbon atoms (O:C), influences the OA hygroscopic growth (Chang et al., 2010;Lambe et al., 2011) which affects CCN activity. In addition, the phase-state changes of SOA during its atmospheric lifetime, which can impact the IN activity, is also influenced by the O:C of the OA (Shiraiwa et al., 2017). Donahue et al. (2011) extended the original one-dimensional VBS framework to two dimensions (2-D VBS) tracking not only the saturation concentration but also the oxygen content of OA during atmospheric transport. This approach further improved the description of the atmospheric evolution of OA and its precursor gases that become increasingly more oxidized, less volatile, and more hygroscopic during their atmospheric aging. However, the large number of additional surrogate organic compounds required by the 2-D VBS framework has hindered implementation in three-dimensional atmospheric models (Napier et al., 2014). Therefore, the 2-D VBS approach has been mostly adopted in box and 1D Lagrangian models (Murphy et al., 2011;Murphy et al., 2012;Chacon-Madrid et al., 2013;Zhao et al., 2015;Paciga et al., 2016). Koo et al. (2014) introduced a hybrid VBS approach for use in three dimensional chemical transport models (CTMs) which combines the simplicity of the VBS

74 with the ability to track the evolution of OA in the 2-D space of volatility and oxygen content.

75 In this work, the computationally efficient module for the description of OA composition and

76 evolution in the atmosphere (ORACLE; Tsimpidi et al., 2014) has been extended to allow for the

77 first time in a global CCM the description of both the volatility and the oxygen content of OA

78 based on the 2-D VBS approach. Similar to ORACLE v1.0, the interface of the new version

79 allows the user to have full control of the complexity of the OA scheme by adjusting the number

80 of species and reactions (i.e., number of compounds, volatility bins, O:C bins) to optimize the

81 computational cost according to the application and the desired chemical resolution. The updated

82 ORACLE module can provide valuable information about the physicochemical evolution of OA

83 during its atmospheric lifetime in support of modeling studies and help quantify the climatic

84 impact of OA.

85

86 **2. Model description**

87 **2.1 EMAC model**

88 The ECHAM/MESSy Atmospheric Chemistry (EMAC) model is a numerical chemistry

89 and climate simulation system that includes sub-models describing lower and middle

90 atmospheric processes and their interaction with oceans, land, and human influences. EMAC

91 consists of the Modular Earth Submodel System and an advanced version of the 5th generation

92 of the European Centre Hamburg (ECHAM) general circulation model. ECHAM5 (Roeckner et

93 al., 2006) serves as the atmospheric dynamic core that simulates the atmospheric flow and is

94 integrated in the base model layer of MESSy. The interface structure of MESSy links the base

95 model with several atmospheric submodels that simulate online the gas-phase chemistry

96 (MECCA; Sander et al., 2011), inorganic aerosol microphysics and dynamics (GMXe; Pringle et

97 al., 2010), organic aerosol formation and growth (ORACLE; Tsimpidi et al., 2014), emissions

98 (ONLEM and OFFLEM; Kerkweg et al., 2006b), dry deposition and sedimentation (DRYDEP

99 and SEDI; Kerkweg et al., 2006a), cloud scavenging (SCAV; Tost et al., 2006), cloud

100 microphysics (CLOUD; Jöckel et al., 2006), and aerosol optical properties (AEROPT; Lauer et

101 al., 2007). EMAC has been extensively described and evaluated against ground-based and

102 satellite observations (Pozzer et al., 2012;Tsimpidi et al., 2014;Tsimpidi et al., 2016,

103 2017;Karydis et al., 2016;Karydis et al., 2017). In this study, the applied spectral resolution of

104 the EMAC model is T63L31, corresponding to a horizontal grid resolution of 1.875^{o}x1.875^{o} and

105   31 vertical layers extending to 18 km altitude (10hPa). EMAC is applied for 11 years covering

106   the period 2000-2010 and the first year is used as spin-up.

107

108   **2.2 ORACLE module**

109   **2.2.1 Module description**

110   ORACLE is a computationally efficient module for the description of organic aerosol

111   composition and evolution in the atmosphere (Tsimpidi et al., 2014) that has been incorporated

112   into the EMAC model. The original version of ORACLE simulated the volatility distribution of a

113   wide variety of semi-volatile organic surrogate compounds using bins of logarithmically spaced

114   effective saturation concentrations. Organic emissions from multiple anthropogenic and natural

115   sources are taken into account using distinct surrogate species for each source category. These

116   surrogates can be subdivided into groups of organic compounds based on their volatility: Low

117   volatility organic compounds (LVOCs, $C* \leq 10^{-2}$ µg m^{-3}), semi-volatile organic compounds,

118   (SVOCs, $10^{-2} < C* \leq 10^2$ µg m^{-3}), intermediate volatility organic compounds (IVOCs, $10^2 < C* \leq$

119   10^6 µg m^{-3}) and volatile organic compounds (VOCs, $C* > 10^6$ µg m^{-3}). These organic compounds

120   are allowed to partition between the gas and aerosol phases resulting in the formation of OA. Gas-

121   phase photochemical reactions that modify the volatility of the organics are taken into account

122   and the oxidation products of each group of precursors are simulated separately in the module to

123   keep track of their origin. The model results for the different organic components in the

124   particulate phase were compared with factor analysis results derived from a comprehensive

125   dataset of aerosol mass spectrometer (AMS) measurements from multiple field campaigns across

126   the Northern Hemisphere. The resulting good agreement between campaign average

127   concentrations and model predictions supports the capability of the model to capture the spatial

128   and temporal characteristics of OA levels. Tsimpidi et al. (2017) conducted an extensive

129   sensitivity analysis of the EMAC OA predictions to uncertain parameters in the ORACLE

130   module. One of the major conclusions of their analysis was that the model performance can be

131   improved by assuming that freshly emitted organic compounds are relatively hydrophobic and

132   become increasingly hygroscopic due to oxidation. As a first step to achieve this goal, the

133   ORACLE module has been further developed here to account for the oxidation state of the

134   organic surrogate compounds. The new version is called ORACLE 2-D.

135

2.2.2. Emission inventory of OA precursors

136

137 The emissions of biogenic VOCs (i.e., isoprene and monoterpenes) are calculated online

138 by EMAC with the ONLEM submodel. The open biomass burning emissions of LVOCs,

139 SVOCs, and IVOCs from savanna and forest fires are based on the Global Fire Emissions

140 Database (GFED version 3.1). The emissions of anthropogenic LVOCs, SVOCs, IVOCs, and

141 VOCs (i.e., aromatics, alkanes, olefins) from fossil and biofuel combustion are derived from the

142 CMIP5 emission inventory for the RCP4.5 scenario. More details about the organic compound

143 emissions used here can be found in Tsimpidi et al. (2014).

144

3 ORACLE 2-D description

3.1 Module overview

147 The original ORACLE v1.0 (called hereafter ORACLE) uses saturation concentration

148 bins to describe the volatility distribution of the major OA components. In this work, ORACLE

149 is extended to also resolve the oxygen content of OA expressed by the O:C ratio. The volatility

150 dimension is discretized in up to 10 logarithmically-spaced volatility bins separating the organic

151 compounds in low volatility (LVOCs, expressed by the volatility bins of 10^{-3}, 10^{-2}, and 10^{-1} μg

152 m^{-3}), semi-volatile (SVOCs, C^* equal to 10^0, 10^1, and 10^2 μg m^{-3}), and those of intermediate

153 volatility (IVOCs, C^* equal to 10^3, 10^4, 10^5 and 10^6 μg m^{-3}). Extremely low volatility organic

154 compounds (ELVOCs, $C^* \leq 10^{-4}$) can be formed by the ozonolysis of monoterpenes and

155 sesquiterpenes (Liggio et al., 2010;Sun et al., 2009) playing an important role for the formation

156 and growth of new particles created in situ in the atmosphere by nucleation (Ehn et al., 2014).

157 The production of ELVOCs from biogenic VOCs is not currently included in ORACLE since the

158 simulation of new particle formation is outside the scope of the current article, and part of work

159 in progress. In addition, the oxygen content dimension is discretized in up to 20 linearly spaced

160 O:C bins subdividing the organic compounds into fresh emissions (expressed by the O:C bins of

161 0.1 and 0.2), less oxygenated organic compounds (O:C equal to 0.3, 0.4, 0.5, and 0.6),

162 moderately oxygenated organic compounds (O:C equal to 0.7, 0.8, 0.9, and 1.0), and highly

163 oxygenated species with O:C>1. The first bin includes also the hydrocarbons with zero oxygen.

164 The O:C range can be extended up to 2 (for CO_2). However, there are only a few atmospheric

165 organic compounds with O:C higher than unity and the observed O:C of ambient OA rarely

166 exceeds 1.1 (Ng et al., 2010; Kroll et al., 2011). The ability of ORACLE v2.0 (called hereafter

167   ORACLE 2-D) to simulate degree of oxidation of OA allows the simulation of its hygroscopicity

168   by using proposed parameterizations that link the hygroscopicity parameter kappa with the O:C

169   of OA (Chang et al., 2010;Lambe et al., 2011;Kuwata and Lee, 2017). In the current application,

170   the hygroscopicity of each OA compound is represented by a linear function of the form

171   κ_{org}=0.18 (O:C) + 0.03 (Lambe et al., 2011). ORACLE 2-D has a flexible interface in which the

172   user can choose the resolution (number of bins used in each dimension) of the 2-D VBS space

173   through a namelist file depending on the desired application and scientific goals. In the rest of

174   this work, we employ ORACLE 2-D using the 2-D VBS at a resolution suitable for medium-term

175   simulations with global chemistry-climate models. This chemical resolution includes 164 organic

176   aerosol surrogate compounds, compared to 34 OA compounds in ORACLE, which result in a

177   16% increase of the EMAC computational burden.

178

179   **3.3 Theory: constructing the two dimensional grid**

180   For the current application, ORACLE 2-D distributes the OA surrogate species into

181   logarithmically spaced volatility bins with C^* varying from 10^{-2} to 10^6 μg m^{-3} and linearly spaced

182   oxygen content bins with O:C varying from 0.1 to 1.2 (Figure 1). Each of the OA surrogate

183   species in this C^*-O:C 2-D space is characterized by a representative number of carbon atoms

184   (n_c) and a molecular weight (MW). Donahue et al. (2011) used structure activity relationships

185   (Pankow and Asher, 2008) to express the C^* as a function of n_c and the number of oxygens per

186   molecule (n_o):

187
$$\log_{10} C^* = 0.475(25 - n_c) - 2.3 n_o + 0.6 \frac{n_c n_o}{n_c + n_o} \quad (1)$$

188

189   Given that n_o is a function of O:C and n_c:

190

191
$$n_o = n_c (\mathrm{O:C}) \quad (2)$$

192

193   n_c can be expressed as a function of C^* and O:C:

194
$$n_C = \frac{11.875 - \log_{10} C^*}{0.475 + 2.3(O:C) - 0.6\dfrac{(O:C)}{1+(O:C)}} \quad (3)$$

195

196 Assuming that the organic compounds consist entirely of carbon, oxygen, and hydrogen atoms

197 (i.e., ignoring nitrogen and sulfur), the *MW* of each surrogate species is a function of the number

198 of carbon (n_C), oxygen (n_O), and hydrogen (n_H) atoms per molecule and therefore it can be

199 calculated as:

200

201
$$MW = n_H + 16n_O + 12n_C \quad (4)$$

202 where,

203

204
$$n_H = n_C(H:C) \quad (5)$$

205

206 H:C is the atomic ratio of hydrogen to carbon approximated by Heald et al. (2010) as:

207

208
$$H:C = 2 - (O:C) \quad (6)$$

209

210 Combining Equations 4, 2, and 5, we get

211

212
$$MW = (15(O:C) + 14)n_C \quad (7)$$

213

214 Given that n_c decreases as C^* increases (Eq. 3), the *MW* calculated by Eq. 7 is consistent with the

215 molecular corridor approach (Shiraiwa et al., 2014) which suggests a tight inverse correlation

216 between volatility and molar mass constrained by boundary lines of low and high O:C ratios.

217   Organic compound emissions from anthropogenic fuel combustion and open biomass

218 burning include LVOCs (with C^* at 298 K equal to 10^{-2} μg m^{-3}) SVOCs (with C^* at 298 K equal

219 to 10^0 and 10^2 μg m^{-3}) and IVOCs (with C^* at 298 K equal to 10^4 and 10^6 μg m^{-3}). Their

220 corresponding emissions are estimated using the emission factors of Tsimpidi et al. (2016).

221   Freshly emitted LVOCs, SVOCs, and IVOCs from anthropogenic and open biomass burning

222   sources are assigned an initial O:C of 0.1 (Figure 1a) and 0.2 (Figure 1b), respectively (Donahue

223   et al., 2011). We distinguish anthropogenic and biogenic VOCs, and their first generation

224   oxidation products are distributed in four volatility bins (with C^* at 298 K equal to 10^0, 10^1, 10^2,

225   and 10^3 µg m^{-3}) by using the aerosol mass yields by Tsimpidi et al. (2014). The O:C distributions

226   of the first generation VOC oxidation products are given by Murphy et al. (2011) and vary with

227   volatility (Figures 1c and 1d).

228

229   **3.4 New photochemical aging scheme**

230   Similar to ORACLE, multiple generations of homogeneous gas-phase reactions with OH

231   are simulated for all OA compounds treated by ORACLE 2-D. After each oxidation step, oxygen

232   atoms are added to the reacting organic gas resulting in an increase of oxygen content and a

233   change of volatility due to functionalization (reducing the volatility) or fragmentation (increasing

234   the volatility). To minimize the computational cost and at the same time simulate the net effect

235   of both fragmentation and functionalization, ORACLE 2-D uses an approach similar to the aging

236   scheme proposed by Murphy et al. (2011). ORACLE 2-D assumes a net average decrease in

237   volatility of aSOA-v reacting with OH by a factor of 10 and the addition of one or two oxygen

238   atoms with the same probability of 50% (Figure 1c). The same addition of oxygen atoms is

239   assumed for bSOA-v, however, its volatility remains unchanged due to a balancing of

240   fragmentation and functionalization effects (Murphy et al., 2012) (Figure 1d). The OH reaction

241   rate constant for both aSOA-v and bSOA-v is 1×10^{-11} cm^3 molecule^{-1} s^{-1} (Tsimpidi et al., 2010).

242   The reaction of SOA-sv and SOA-iv with OH with a rate constant of 2×10^{-11} cm^3 molecule^{-1} s^{-1}

243   (Tsimpidi et al., 2014) results in the addition of two or three oxygen atoms (with equal

244   probability) and the reduction of their volatilities by a factor of 100 (Figure 1a, 1b). The number

245   of added oxygen atoms (n_{o_+}) due to the reaction with OH is then expressed as an increase of

246   O:C in the 2-D space. Each of the OA surrogate compounds in the 2-D space described in

247   Section 3.3 has a representative number of carbon per molecule (n_c). Assuming that carbon is

248   conserved during the reaction with OH, the O:C of the product is calculated as follows:

249

250
$$(O:C)_{product} = (O:C)_{reactant} + \frac{n_{O+}}{n_C} \quad (8)$$

251

252 If the $(O:C)_{product}$ has more than one decimal places, then is distributed between the two adjacent

253 O:C bins of the 2-D space by using linear interpolation. Finally, since carbon is conserved, the

254 increase in mass due to the added oxygen after each oxidation reaction is calculated as:

255

256
$$\frac{OM_{product}}{OM_{reactant}} = \frac{\left(\frac{OM}{OC}\right)_{product}}{\left(\frac{OM}{OC}\right)_{reactant}} \quad (9)$$

257

258 where, following Murphy et al. (2011),

259

260
$$\left(\frac{OM}{OC}\right) = 1 + 16(O:C) + \frac{1}{12}(H:C) \quad (10)$$

261

262 **3.5 Phase partitioning calculations**

263   ORACLE 2-D uses the core layer of the ORACLE module to calculate the partitioning of

264 organic compounds between the gas and particle phases by assuming bulk equilibrium (Tsimpidi

265 et al., 2014). However, the computational time required for the phase partitioning increases

266 super-linearly with the number of species. As the condensation/evaporation of organic

267 compounds depends only on their saturation concentration and not their O:C ratio, only one

268 equilibrium calculation is performed per volatility bin of each category (i.e., fuel combustion,

269 biomass burning, anthropogenic VOC products, and biogenic VOC products). This approach

270 reduces significantly the number of equation to be solved and the corresponding computational

271 cost of the phase partitioning calculations.

272   The ORACLE core layer calculates the aerosol composition at equilibrium by solving the

273 following set of *n* nonlinear equations:

274

275
$$C_{a,i} = C_{t,i} - x_i C_i^* \quad \text{for } i = 1, n \qquad (11)$$

276

277
$$x_i = \frac{C_{a,i}/M_i}{\sum\limits_{i=1}^{n} C_{a,i}/M_i} \qquad (12)$$

278

279 where $C_{t,i}$ and $C_{a,i}$ are the total and aerosol-phase concentrations of product i in µg m^{-3},

280 respectively, C_i^* is the effective saturation concentration of species i, x_i is the mole fraction of

281 product i in the absorbing organic phase, and M_i is the molecular weight of product i which

282 corresponds to the weighted average molecular weight of the species with the same saturation

283 concentration.

284 Assuming that the distribution of the species of the same volatility bin in the different O:C

285 bins does not change due to the condensation or evaporation, the gas and aerosol concentrations

286 of each compound in the 2-D space after the phase partitioning calculations are given by:

287

288
$$SOG_{i,j}(t + \Delta t) = \left(\sum\limits_{j=1}^{m} SOG_{i,j}(t + \Delta t) \right) \frac{SOG_{i,j}(t) + SOA_{i,j}(t)}{\sum\limits_{j=1}^{m} SOG_{i,j}(t) + \sum\limits_{j=1}^{m} SOA_{i,j}(t)} \qquad (13)$$

289
290 and
291

292
$$SOA_{i,j}(t + \Delta t) = \left(\sum\limits_{j=1}^{m} SOA_{i,j}(t + \Delta t) \right) \frac{SOG_{i,j}(t) + SOA_{i,j}(t)}{\sum\limits_{j=1}^{m} SOG_{i,j}(t) + \sum\limits_{j=1}^{m} SOA_{i,j}(t)} \qquad (14)$$

293

294 where, SOG and SOA are the gas and aerosol concentrations of each compound, respectively, i

295 and j are the volatility and O:C bins index in the 2-D space, respectively, m is the total number of

296 O:C bins, and t and $t+\Delta t$ are the times before and after the phase partitioning calculations,

297 respectively.

298

299

4. Model results

4.1 Total OA and O:C

Simulated total OA concentrations are high over regions affected by anthropogenic fuel combustion and open biomass burning (Figure 2). The highest annual average OA concentrations at the surface are predicted over the densely populated areas of Eastern China, Northern India and Bangladesh (10-28 μg m^{-3}), as well as over the tropical forest in the Congo Basin (12-22 μg m^{-3}). Considerably high OA concentrations are also predicted over the tropical forests of Southeast Asia and the Amazon (6-17 μg m^{-3}). Strong fossil fuel combustion sources over the Arabian Peninsula result in annual average OA concentrations of 6-10 μg m^{-3}. Over Europe, predicted OA annual average concentrations at the ground level are in the 3-7 μg m^{-3} range. Over North America, the highest OA concentration is simulated over Southern California, and also over the Mexico City metropolitan area, and the Southeastern USA (2-8 μg m^{-3}). OA concentrations in the 0.5-1 μg m^{-3} range are predicted over parts of the oceans due to the long-range transport of OA from the adjacent continental sources. The calculated total tropospheric OA burden is 3.3 Tg, which is higher compared to the calculated tropospheric burden of ORACLE v1.0 (2 Tg; Tsimpidi et al., 2016) but is within the range of OA tropospheric burdens (0.7 to 3.8 Tg) from 31 global CTMs reported by Tsigaridis et al. (2014).

Figure 3a depicts the annual average simulated O:C ratio of total OA at the surface. Lower values of O:C are predicted close to OA sources, i.e., over the industrialized areas of the Northern Hemisphere, and over the tropical and boreal forests. The lowest average values occur over the boreal forests (as low as 0.3) due to the limited photochemical activity over these regions, in contrast to the tropical forests, where O:C is around 0.5. Over the densely populated areas of Asia, Europe and North America, the O:C is about 0.3-0.4, i.e., close to the anthropogenic sources. O:C levels increase rapidly (in excess of 0.6) downwind of the sources due to photochemical aging of the transported OA. The highest O:C values are calculated over the Sahara Desert and the remote Atlantic and Pacific Oceans (0.8-1), however, over these regions, OA concentrations are low (Figure 2). O:C ratios increase significantly with altitude according to the model (Figure 3b) since organic vapors transported vertically react with OH, forming products with higher oxygen content. Over the mid-latitudes of the Northern Hemisphere, the average O:C ratio near the surface is 0.55, and increases as the air masses are transported aloft by approximately 0.05 for every 100 hPa (Figure 3b).

331

4.2 POA and SOA

332

333   Figure 4a depicts the decadal average simulated POA concentrations at the surface. POA

334   concentrations are high over the densely populated areas of the Northern Hemisphere due to

335   strong fuel combustion emissions from the industrial, energy, residential and transport sectors.

336   The highest concentrations are calculated over Eastern China (3-13 μg m^{-3}), Bangladesh (2-8 μg

337   m^{-3}), and Eastern Europe (1-3 μg m^{-3}). Open biomass burning emissions from forest, woodland,

338   peatland and savannah fires result in high POA concentrations over the tropics (3-8 μg m^{-3} over

339   the Congo Basin) and the boreal forests (1-6 μg m^{-3} over Russia). However, a large fraction of

340   POA evaporates due to dilution as the air masses travel downwind from the sources, resulting in

341   significant reduction of the concentration (Figure 4a). Then, the material that is transferred to the

342   gas phase can be oxidized and recondense to the aerosol phase forming SOA that persists even

343   far from the sources (Figure 4b). This results in a relatively homogeneous regional distribution

344   of SOA with a continental background of 2 μg m^{-3} and high concentrations even far downwind

345   from anthropogenic (e.g., 7-22 μg m^{-3} over South and Eastern Asia) and open biomass burning

346   (e.g., 9-17 μg m^{-3} over Central Africa) sources. Lower concentrations are predicted over the

347   boreal forests (~1 μg m^{-3}) due to minor photochemical activity.

348   The calculated tropospheric burden of POA and SOA is 0.25 Tg and 3.05 Tg,

349   respectively. While the value of POA is very similar to the corresponding tropospheric burden of

350   ORACLE v1.0 (0.24 Tg), the tropospheric burden of SOA has increased significantly (1.74 Tg in

351   ORACLE v1.0). The tropospheric burden of POA calculated by ORACLE 2-D is much lower

352   than most global CTMs in the AEROCOM intercomparison study (mean value of 0.85 Tg)

353   (Tsigaridis et al., 2014). This difference is due to the evaporation of POA and its conversion into

354   SOA in ORACLE 2-D, given that this dynamic behavior of POA is not taken into account by

355   most of the global CTMs. On the other hand, the ORACLE 2-D calculated SOA tropospheric

356   burden is higher than most CTMs from the AEROCOM intercomparison study (mean value of 1

357   Tg) (Tsigaridis et al., 2014) due to its stronger chemical production. As indicated by Tsimpidi et

358   al. (2016), the POA burden is underestimated by our model, especially in the urban environment

359   in the winter, because our emission inventory does not yet account for residential wood burning

360   (Denier van der Gon et al., 2015).

361

362 **4.3 Fresh and Aged SOA**

363   The major advantage, at least in this initial phase, of extending the ORACLE module to

364 describe the oxygen content of OA is the model's ability to quantify the degree of photochemical

365 processing of the OA. The model can distinguish the fresh SOA that is relatively less oxygenated

366 and the highly aged and oxygenated SOA. As a first approximation, OA compounds with O:C ≤

367 0.6 are considered "fresh SOA" and OA compounds with O:C > 0.6 are considered as "aged

368 SOA".

369   Figure 5 depicts the average concentrations of fresh and aged SOA and their fractional

370 contributions to total SOA at the surface. Fresh SOA exceeds aged SOA close to the source areas

371 (Figures 5c). On the other hand, the spatial distribution of aged SOA extends further from the

372 sources with relatively high concentrations even over remote continental (e.g., Sahara) and

373 oceanic (e.g., North Pacific) regions (Figure 5b). The fraction of aged SOA is higher over the

374 industrialized regions (0.4-0.7), where IVOCs comprise 70% of total fuel combustion emissions,

375 and lower over the tropics (0.1-0.5), where IVOCs represent 40% of total open biomass burning

376 emissions (Figure 5d). Overall, the tropospheric burden of fresh SOA is 1.26 Tg and of aged

377 SOA 1.79 Tg.

378   The simulated vertical profiles of fresh and aged SOA are quite different (Figure 6). Both

379 fresh and aged SOA concentrations are high near the surface with zonal averages of 0.9-1.7 μg

380 m^{-3} over the northern mid-latitudes and the tropics. However, at higher altitudes the oxidation of

381 fresh SOA continues, which leads to the transformation into aged SOA. Therefore, above 960

382 hPa altitude the zonal average concentrations of fresh SOA decrease gradually (below 1 μg m^{-3})

383 and that of aged SOA increase, exceeding in some cases 1.5 μg m^{-3} at 850 hPa altitude. Further

384 aloft in the atmosphere (above 700 hPa altitude) the levels of both fresh and aged SOA are

385 reduced significantly due to dilution and removal.

386

387 **4.3 2-D space distribution**

388 In this section, we present a new feature that comes along with the upgraded ORACLE 2-D.

389 Since ORACLE 2-D explicitly describes the concentration of organic surrogate species in two

390 dimensional space, defined by their volatility and O:C ratio, it can also provide as output their

391 distribution in this 2-D space. As an example, Figure 7 depicts the 2-D distribution of the

392 average total OA concentrations during the years 2001-2010 over central Europe and the

393 Amazon basin. The first left column represents all the species with $C^*\leq10^{-2}$ µg m^{-3}, while the top

394 line represents all the species with O:C ≥ 1.2.

395 Over Europe, approximately 50% of OA has $C^* = 1$ µg m^{-3}. About 10% of the OA is

396 emitted directly in this volatility bin as POA with O:C = 0.1, while the rest, 40%, is SOA with

397 higher O:C from the aging of more volatile compounds. The volatility bin with $C^* = 10^{-2}$ µg m^{-3}

398 is also important, containing 18% of the total OA. On the other hand, volatility bins with $C^* >$

399 10^2 contain less than 1% of total OA since organic species in these high volatility bins exist

400 mainly in the gas phase. Furthermore, about 30% of the total OA over Europe has O:C≤0.2,

401 mainly from direct emissions of POA from fuel combustion sources with O:C=0.1 (20% of total

402 OA). Organic species with O:C = 0.4 are also important, representing 15% of the total OA.

403 Overall, 40% of OA over Europe has 0.3≤O:C≤ 0.6 and 30% is highly oxidized with O:C≥0.7.

404 Over the Amazon, similar to Europe, approximately 50% of total OA has $C^* = 1$ µg m^{-3}

405 while bins with $C^* > 10^2$ contain only 2% of total OA. However, volatility bins with $10^2 \leq C^*$

406 $\leq 10^3$ are more important compared to Europe containing about 30% of the total OA

407 concentrations. This discrepancy can be attributed to the high bSOA-v concentrations over the

408 Amazon rainforest, which remain within higher volatility bins during their photochemical aging

409 compared to aSOA-v. Furthermore, similar to Europe, about 30% of total OA over the Amazon

410 has O:C ≤ 0.2, mainly affected by the direct aerosol emissions from biomass burning with O:C =

411 0.2 (~20% of total OA). OA species with 0.3≤O:C≤0.6 represent 55% of the total OA with

412 mostly O:C = 0.4 (35% of total OA). On the other hand, only 15% of the total OA is highly

413 oxidized with O:C ≥ 0.7. Comparing these results to Europe shows that OA over biomass

414 burning areas (e.g., the Amazon) are estimated to be less oxidized than OA over anthropogenic

415 areas (e.g., Europe).

416

417 **5. Model performance evaluation**

418 The mean absolute gross error (MAGE), mean bias (MB), normalized mean error (NME),

419 normalized mean bias (NMB), and the root mean square error (RMSE) are used to assess the

420 model performance of the simulations of OA components (i.e., POA, fresh and aged SOA) and

421 O:C:

422

$$MAGE = \frac{1}{N} \sum_{i=1}^{N} \left| P_i - O_i \right| \quad (15) \qquad MB = \frac{1}{N} \sum_{i=1}^{N} \left(P_i - O_i \right) \quad (16)$$

$$NME = \frac{\sum_{i=1}^{N} \left| P_i - O_i \right|}{\sum_{i=1}^{N} O_i} \quad (17) \qquad NMB = \frac{\sum_{i=1}^{N} \left(P_i - O_i \right)}{\sum_{i=1}^{N} O_i} \quad (18)$$

$$RMSE = \left[\frac{1}{N} \sum_{i=1}^{N} \left(P_i - O_i \right)^2 \right]^{\frac{1}{2}} \quad (19)$$

where O_i is the observed campaign average value of the ith OA component or O:C, P_i is the corresponding modelled value during the same period, and N is the total number of comparisons used for the evaluation.

5.1 Organic aerosol concentrations

The simulated POA and SOA can be compared against AMS factor analysis results from 61 field campaigns performed during the period 2001–2010 over urban-downwind and rural environments in the Northern Hemisphere (Figure 8). Information for each of these campaigns is given in Tsimpidi et al. (2016). Factor-analysis techniques classify OA into hydrocarbon-like OA (HOA), biomass burning OA (BBOA), and oxygenated OA (OOA). HOA is assumed to correspond to POA from fossil fuel combustion, and BBOA corresponds to POA from biomass burning (Crippa et al., 2014). Therefore, simulated POA is compared here against the sum of AMS HOA and BBOA (Table 1). OOA corresponds to modelled SOA (Table 2) and can be further classified into two subtypes, semi-volatile OOA (SVOOA) and low volatility OOA (LVOOA) (Crippa et al., 2014). Recent studies have suggested that the main difference between these two OOA types is often not so much their volatility, but mostly their oxygen content (Kostenidou et al., 2016; Louvaris et al., 2017). These two OOA types represent distinct oxidation states with O:C of 0.33-0.67 for SVOOA and 0.67-1.00 for LVOOA (Donahue et al., 2012). Therefore, SVOOA can be compared at least as a zero-order approximation against the simulated fresh SOA (Table 3) and LVOOA against the simulated aged SOA (Table 4).

449   The model reproduces the observed campaign average POA concentrations well in most cases

450   over both the urban downwind and rural locations (Table 1, Figure 8a). The average simulated

451   POA concentration over the urban downwind regions is around 0.65 μg m^{-3} and it decreases

452   further after continued transport from the sources to 0.45 μg m^{-3} over the rural areas. Compared

453   to AMS HOA concentrations, modelled POA is unbiased over rural environments, however, it is

454   underestimated downwind of urban areas, as indicated in Sect. 4.2 (MB=-0.17 μg m^{-3}). The

455   model has the best performance during summer with MB=-0.05 μg m^{-3} and RMSE = 0.40 μg

456   m^{-3}. Compared to ORACLE (Tsimpidi et al., 2016), ORACLE 2-D produces almost identical

457   concentrations of POA, hence the model performance is unchanged.

458   Calculated SOA concentrations are higher than POA both downwind of major urban

459   centers (2.76 μg m^{-3}) and rural locations (2.53 μg m^{-3}). Simulated average SOA concentrations

460   are slightly low-biased compared to AMS OOA measurements downwind of urban areas (MB=-

461   0.22 μg m^{-3}) and over rural areas (MB=-0.18 μg m^{-3}). While the model performs well during

462   spring (NMB=10%), summer (NMB=-10%), and autumn (NMB=0%), it strongly underestimates

463   SOA concentrations during winter (NMB=-76%). This underestimation of SOA by the model is

464   mostly due to missing LVOOA. For the 41 campaigns in which both OOA types were identified,

465   EMAC reproduces the fresh SOA concentrations well (compared to SVOOA) with a MB of 0.41

466   and 0.32 μg m^{-3} downwind of urban and in rural locations, respectively (Table 4). Furthermore,

467   except during winter, the model is also able to capture the seasonal variations of the fresh SOA

468   concentration (Table 4). However, the model underpredicts the aged SOA concentrations

469   (compared to AMS measured LVOOA) with a MB of -0.95 and -0.70 μg m^{-3} over urban

470   downwind and rural locations, respectively. This aged SOA underestimation is also evident

471   during the four seasons of the year and especially during winter (NMB = -93%). This result may

472   indicate that the model underestimates the atmospheric aging rate of SOA or misses processes

473   forming highly oxidized OA, e.g., highly oxidized ELVOCs from the ozonolysis of terpenes

474   (Ehn et al., 2014; Jokinen et al., 2016). Another useful feature of ORACLE 2-D is that detailed

475   AMS measurements can be used to gain further insights into what causes biases and errors in its

476   OA predictions. Compared to ORACLE (Tsimpidi et al., 2016), ORACLE 2-D tends to produce

477   higher fresh SOA concentrations and slightly lower aged SOA concentrations. However, this

478   discrepancy may be partially due to the fact that in ORACLE fresh SOA is assumed to

479   correspond only to first generation oxidation products, while in ORACLE 2-D fresh SOA is

480 defined based on the O:C ratio, and includes higher generation oxidation products as well.

481 Overall, the simulated average total SOA concentrations in ORACLE 2-D (2.59 μg m^{-3}) are

482 higher than ORACLE (1.91 μg m^{-3}) reducing the gap with the corresponding AMS OOA (2.78

483 μg m^{-3}).

484

485 **5.2 O:C ratio**

486   The simulated O:C ratio of total OA and SOA is compared against observed O:C of OA

487 and OOA from 30 and 58 field campaigns, respectively, performed during the period 2001–2010

488 in the Northern Hemisphere (Tables 5, 6). Given that global models, including EMAC,

489 underestimate concentrations of POA and SOA over urban locations (Tsigaridis et al., 2014;

490 Tsimpidi et al., 2016), AMS data from these locations is not included for the statistical

491 evaluation of the calculated O:C (Figure 9, Tables 7, 8). In fact, the model tends to overestimate

492 the O:C of total OA compared to observations from urban locations (e.g., Mexico City,

493 Barcelona, New York, Riverside, Paris; Table 5). This overprediction can be attributed to the

494 coarse spatial resolution and the difficulty to represent freshly emitted (or formed) OA on a local

495 scale. On the other hand, the model performs remarkably well in reproducing the O:C ratio of

496 both total OA (NMB=7%, RMSE=0.13) and SOA (NMB=5%, RMSE=0.12) in non-urban areas.

497   The model tends to overestimate the O:C ratio of total OA compared to observations

498 from field campaigns close to the coasts (e.g., western coast of Chile, Mace Head). The model

499 reproduces very well the low O:C ratios of total OA during winter and the higher values during

500 spring and autumn (Table 7). On the other hand, it overestimates the O:C of total OA during

501 summer (MB=0.14). However, there are only 4 field campaigns conducted during the summer

502 months that provide O:C of total OA with surprisingly low O:C values for this time of the year

503 (0.3-0.4) which are not captured by the model. Overall, the O:C of total OA is slightly

504 overestimated by the model (MB=0.04).

505   Simulated O:C of SOA is relatively high (0.5-0.7) at most observational sites, which

506 agrees well with measurements. The model also captures the very high O:C values (larger than

507 0.7) observed over very remote areas (e.g., Okinawa, Finokalia). On the other hand, low O:C

508 ratios (lower than 0.5), reported by a few field campaigns, are overestimated by the model (Duke

509 forest, Rhine Valley, Jiaxing). Remarkably, the model performance during winter is unbiased for

510 the O:C ratio of SOA (Table 8). This is in contrast to its inability to reproduce SOA

511 concentrations during winter (Tsimpidi et al., 2016). During the other seasons the model slightly

512 overestimates the O:C ratio of SOA with an MB ranging from 0.02 (during spring) to 0.07

513 (during summer and autumn).

514

515 **6. Conclusions**

516   The ORACLE module for the description of OA composition and evolution in the

517 atmosphere (Tsimpidi et al., 2014) has been extended to simultaneously simulate the volatility

518 and the oxygen content of OA that results from atmospheric aging. Similar to ORACLE v1.0, the

519 new version is implemented in the EMAC CCM, and considers the formation of OA from the

520 emissions and chemical aging of LVOCs, SVOCs and IVOCs from fossil fuel, biofuel and

521 biomass burning related sources, as well as from the oxidation of anthropogenic and biogenic

522 VOC precursors. The updated ORACLE module employs the 2-D VBS framework that uses

523 logarithmically spaced effective saturation concentration bins to describe the volatility of organic

524 compounds, and linearly spaced oxygen per carbon ratio bins to describe their oxygenation state.

525   The simulated concentrations of OA and its components (i.e., POA and SOA) are similar

526 to ORACLE v1.0 with relatively high concentrations over the industrialized areas in the

527 Northern Hemisphere and the biomass burning areas in the tropics. The tropospheric burdens of

528 POA and SOA are calculated to be 0.25 and 3.05 Tg respectively, the latter being higher than

529 with ORACLE v1.0. The new ORACLE 2-D module additionally allows calculation of the

530 oxidation state of OA (in terms of O:C), and therefore, its classification into fresh SOA (with

531 O:C lower than 0.6) and aged SOA (with O:C higher than 0.6). O:C is calculated to be relatively

532 low close to source regions and at high latitudes. The predicted O:C ratio is as low as 0.3 over

533 the boreal forests, 0.3-0.4 close to the anthropogenic sources in the Northern Hemisphere, 0.5

534 over the tropical forests and higher than 0.6 downwind of source areas and at altitudes aloft.

535 Accordingly, fresh SOA concentrations are higher close to sources while aged SOA increases as

536 the air masses are transported away from the sources and to higher altitudes. The estimated

537 tropospheric burden of fresh SOA is 1.26 Tg and of aged SOA 1.79 Tg. The analysis of model

538 results regarding the distribution of OA in the 2-D space of volatility and oxygen content showed

539 that half of OA has $C^* = 1$ µg m^{-3} over both anthropogenic areas (e.g., Europe) and tropical

540 forests (e.g., Amazon). Furthermore, over Europe OA compounds are more strongly oxidized

541 than over the Amazon, and consist of 40% fresh OA and 30% aged SOA (compared to 55% and

542   15%, respectively, over the Amazon). The remainder 30% in both areas consists of POA or very

543   low oxidized material with O:C≤0.2.

544   The simulated OA components (POA, fresh, aged and total SOA) have been compared

545   with observed subtypes of OA (sum of HOA and BBOA, SVOOA, LVOOA and OOA) derived

546   from AMS factor analysis results from 61 field campaigns, performed during the period 2001–

547   2010 over urban-downwind and rural environments in the Northern Hemisphere. The model

548   reproduces the POA concentrations over both types of environment with low bias. While the

549   model appears to capture the fresh SOA concentrations reasonably well, it underestimates the

550   concentrations of aged SOA, resulting in an overall underprediction of total SOA. The

551   underestimation of aged SOA by the model emphasizes the need to better describe chemical

552   aging processes and further explore the effect of ELVOCs on the formation of SOA.

553   Furthermore, the model realistically reproduces the observed O:C ratio of total OA (NMB=7%)

554   and OOA (NMB=5%) from 50 field campaigns over urban-downwind and rural areas.

555   ORACLE 2-D is a flexible module that efficiently describes the organic aerosol

556   composition and evolution in the atmosphere by simulating the changes in OA volatility and

557   oxygen content throughout its lifetime in the atmosphere. The ability of ORACLE 2-D to

558   simulate the degree of OA oxidation can help determine the changing OA hygroscopicity during

559   atmospheric aging. ORACLE 2-D can potentially provide valuable insights into the composition

560   and reactivity of OA and the physicochemical evolution during atmospheric transport of OA,

561   which can help reduce aerosol-related uncertainties that persist in global atmospheric chemistry

562   and climate modeling.

563

564   **Code and Data Availability**

565   To use ORACLE 2-D as part of EMAC, please first apply for an ECHAM5 and a MESSy

566   license. The GCM ECHAM5 has been developed at the Max Planck Institute for Meteorology in

567   Hamburg   (see: www.mpimet.mpg.de/en/wissenschaft/modelle/echam/echam5.html).   The

568   Modular Earth Submodel System (MESSy) is developed and applied by a consortium of

569   institutions, initiated by the Max Planck Institute for Chemistry. The usage of MESSy and access

570   to the source code is licensed to all affiliates of institutions that are members of the MESSy

571   Consortium. Institutions can be a member of the MESSy Consortium by signing the MESSy

572   Memorandum of Understanding. More information can be found on the MESSy Consortium

573 Website (www.messy-interface.org). The measurement data used for the evaluation of the model

574 can be found in Tables 5 and 6 of this manuscript and Tables S6 and S7 in the supplement of

575 Tsimpidi et al. (2016) (available online at https://doi.org/10.5194/acp-16-8939-2016-

576 supplement).

577

578 **Acknowledgements**

579   A.P. Tsimpidi acknowledges support from a DFG individual grand programme (project

580 reference TS 335/2-1) and V.A. Karydis acknowledges support from a FP7 Marie Curie Career

581 Integration Grant (project reference 618349).

582

583 **References**

584 Ahmadov, R., McKeen, S. A., Robinson, A. L., Bahreini, R., Middlebrook, A. M., de Gouw, J.
585   A., Meagher, J., Hsie, E. Y., Edgerton, E., Shaw, S., and Trainer, M.: A volatility basis
586   set model for summertime secondary organic aerosols over the eastern United States in
587   2006, J. Geophys. Res. Atmos., 117, 10.1029/2011jd016831, 2012.
588 Aiken, A. C., Decarlo, P. F., Kroll, J. H., Worsnop, D. R., Huffman, J. A., Docherty, K. S.,
589   Ulbrich, I. M., Mohr, C., Kimmel, J. R., Sueper, D., Sun, Y., Zhang, Q., Trimborn, A.,
590   Northway, M., Ziemann, P. J., Canagaratna, M. R., Onasch, T. B., Alfarra, M. R., Prevot,
591   A. S. H., Dommen, J., Duplissy, J., Metzger, A., Baltensperger, U., and Jimenez, J. L.:
592   O/C and OM/OC ratios of primary, secondary, and ambient organic aerosols with high-
593   resolution time-of-flight aerosol mass spectrometry, Environmen. Sci. & Technol., 42,
594   4478-4485, 2008.
595 Allan, J. D., Williams, P. I., Morgan, W. T., Martin, C. L., Flynn, M. J., Lee, J., Nemitz, E.,
596   Phillips, G. J., Gallagher, M. W., and Coe, H.: Contributions from transport, solid fuel
597   burning and cooking to primary organic aerosols in two UK cities, Atmospheric
598   Chemistry and Physics, 10, 647-668, 10.5194/acp-10-647-2010, 2010.
599 Athanasopoulou, E., Vogel, H., Vogel, B., Tsimpidi, A. P., Pandis, S. N., Knote, C., and
600   Fountoukis, C.: Modeling the meteorological and chemical effects of secondary organic
601   aerosols during an EUCAARI campaign, Atmos. Chem. Phys., 13, 625-645, 2013.
602 Carbone, S., Aurela, M., Saarnio, K., Saarikoski, S., Timonen, H., Frey, A., Sueper, D., Ulbrich,
603   I. M., Jimenez, J. L., Kulmala, M., Worsnop, D. R., and Hillamo, R. E.: Wintertime
604   Aerosol Chemistry in Sub-Arctic Urban Air, Aerosol Science and Technology, 48, 313-
605   323, 10.1080/02786826.2013.875115, 2014.
606 Chacon-Madrid, H. J., Henry, K. M., and Donahue, N. M.: Photo-oxidation of pinonaldehyde at
607   low NOx: from chemistry to organic aerosol formation, Atmospheric Chemistry and
608   Physics, 13, 3227-3236, 10.5194/acp-13-3227-2013, 2013.
609 Chang, R. Y. W., Slowik, J. G., Shantz, N. C., Vlasenko, A., Liggio, J., Sjostedt, S. J., Leaitch,
610   W. R., and Abbatt, J. P. D.: The hygroscopicity parameter (kappa) of ambient organic
611   aerosol at a field site subject to biogenic and anthropogenic influences: relationship to

612   degree of aerosol oxidation, Atmospheric Chemistry and Physics, 10, 5047-5064,
613   10.5194/acp-10-5047-2010, 2010.
614 Ciarelli, G., El Haddad, I., Bruns, E., Aksoyoglu, S., Mohler, O., Baltensperger, U., and Prevot,
615   A. S. H.: Constraining a hybrid volatility basis-set model for aging of wood-burning
616   emissions using smog chamber experiments: a box-model study based on the VBS
617   scheme of the CAMx model (v5.40), Geoscientific Model Development, 10, 2303-2320,
618   10.5194/gmd-10-2303-2017, 2017.
619 Crippa, M., El Haddad, I., Slowik, J. G., DeCarlo, P. F., Mohr, C., Heringa, M. F., Chirico, R.,
620   Marchand, N., Sciare, J., Baltensperger, U., and Prevot, A. S. H.: Identification of marine
621   and continental aerosol sources in Paris using high resolution aerosol mass spectrometry,
622   Journal of Geophysical Research-Atmospheres, 118, 1950-1963, 10.1002/jgrd.50151,
623   2013.
624 Docherty, K. S., Aiken, A. C., Huffman, J. A., Ulbrich, I. M., DeCarlo, P. F., Sueper, D.,
625   Worsnop, D. R., Snyder, D. C., Peltier, R. E., Weber, R. J., Grover, B. D., Eatough, D. J.,
626   Williams, B. J., Goldstein, A. H., Ziemann, P. J., and Jimenez, J. L.: The 2005 Study of
627   Organic Aerosols at Riverside (SOAR-1): instrumental intercomparisons and fine particle
628   composition, Atmospheric Chemistry and Physics, 11, 12387-12420, 10.5194/acp-11-
629   12387-2011, 2011.
630 Donahue, N. M., Robinson, A. L., Stanier, C. O., and Pandis, S. N.: Coupled partitioning,
631   dilution, and chemical aging of semivolatile organics, Environ. Sci. Technol., 40, 2635-
632   2643, 2006.
633 Donahue, N. M., Epstein, S. A., Pandis, S. N., and Robinson, A. L.: A two-dimensional volatility
634   basis set: 1. organic-aerosol mixing thermodynamics, Atmos. Chem. and Phys., 11, 3303-
635   3318, 2011.
636 Ehn, M., Thornton, J. A., Kleist, E., Sipila, M., Junninen, H., Pullinen, I., Springer, M., Rubach,
637   F., Tillmann, R., Lee, B., Lopez-Hilfiker, F., Andres, S., Acir, I.-H., Rissanen, M.,
638   Jokinen, T., Schobesberger, S., Kangasluoma, J., Kontkanen, J., Nieminen, T., Kurten,
639   T., Nielsen, L. B., Jorgensen, S., Kjaergaard, H. G., Canagaratna, M., Maso, M. D.,
640   Berndt, T., Petaja, T., Wahner, A., Kerminen, V.-M., Kulmala, M., Worsnop, D. R.,
641   Wildt, J., and Mentel, T. F.: A large source of low-volatility secondary organic aerosol,
642   Nature, 506, doi: 10.1038/nature13032, 2014.
643 Fountoukis, C., Megaritis, A. G., Skyllakou, K., Charalampidis, P. E., Pilinis, C., van der Gon,
644   H., Crippa, M., Canonaco, F., Mohr, C., Prevot, A. S. H., Allan, J. D., Poulain, L., Petaja,
645   T., Tiitta, P., Carbone, S., Kiendler-Scharr, A., Nemitz, E., O'Dowd, C., Swietlicki, E.,
646   and Pandis, S. N.: Organic aerosol concentration and composition over Europe: insights
647   from comparison of regional model predictions with aerosol mass spectrometer factor
648   analysis, Atmospheric Chemistry and Physics, 14, 9061-9076, 10.5194/acp-14-9061-
649   2014, 2014.
650 Gao, C. Y., Tsigaridis, K., and Bauer, S. E.: MATRIX-VBS (v1.0): implementing an evolving
651   organic aerosol volatility in an aerosol microphysics model, Geoscientific Model
652   Development, 10, 751-764, 10.5194/gmd-10-751-2017, 2017.
653 Ge, X. L., Setyan, A., Sun, Y. L., and Zhang, Q.: Primary and secondary organic aerosols in
654   Fresno, California during wintertime: Results from high resolution aerosol mass
655   spectrometry, Journal of Geophysical Research-Atmospheres, 117,
656   10.1029/2012jd018026, 2012.

657 Gong, Z. H., Lan, Z. J., Xue, L., Zeng, L. W., He, L. Y., and Huang, X. F.: Characterization of
658   submicron aerosols in the urban outflow of the central Pearl River Delta region of China,
659   Frontiers of Environmental Science & Engineering, 6, 725-733, 10.1007/s11783-012-
660   0441-8, 2012.
661 Guo, H. Y., Liu, J. M., Froyd, K. D., Roberts, J. M., Veres, P. R., Hayes, P. L., Jimenez, J. L.,
662   Nenes, A., and Weber, R. J.: Fine particle pH and gas-particle phase partitioning of
663   inorganic species in Pasadena, California, during the 2010 CalNex campaign,
664   Atmospheric Chemistry and Physics, 17, 5703-5719, 10.5194/acp-17-5703-2017, 2017.
665 Hawkins, L. N., Russell, L. M., Covert, D. S., Quinn, P. K., and Bates, T. S.: Carboxylic acids,
666   sulfates, and organosulfates in processed continental organic aerosol over the southeast
667   Pacific Ocean during VOCALS-REx 2008, Journal of Geophysical Research-
668   Atmospheres, 115, 10.1029/2009jd013276, 2010.
669 Hayes, P. L., Ortega, A. M., Cubison, M. J., Froyd, K. D., Zhao, Y., Cliff, S. S., Hu, W. W.,
670   Toohey, D. W., Flynn, J. H., Lefer, B. L., Grossberg, N., Alvarez, S., Rappenglueck, B.,
671   Taylor, J. W., Allan, J. D., Holloway, J. S., Gilman, J. B., Kuster, W. C., De Gouw, J. A.,
672   Massoli, P., Zhang, X., Liu, J., Weber, R. J., Corrigan, A. L., Russell, L. M., Isaacman,
673   G., Worton, D. R., Kreisberg, N. M., Goldstein, A. H., Thalman, R., Waxman, E. M.,
674   Volkamer, R., Lin, Y. H., Surratt, J. D., Kleindienst, T. E., Offenberg, J. H., Dusanter, S.,
675   Griffith, S., Stevens, P. S., Brioude, J., Angevine, W. M., and Jimenez, J. L.: Organic
676   aerosol composition and sources in Pasadena, California, during the 2010 CalNex
677   campaign, Journal of Geophysical Research-Atmospheres, 118, 9233-9257,
678   10.1002/jgrd.50530, 2013.
679 He, L. Y., Huang, X. F., Xue, L., Hu, M., Lin, Y., Zheng, J., Zhang, R. Y., and Zhang, Y. H.:
680   Submicron aerosol analysis and organic source apportionment in an urban atmosphere in
681   Pearl River Delta of China using high-resolution aerosol mass spectrometry, Journal of
682   Geophysical Research-Atmospheres, 116, 10.1029/2010jd014566, 2011.
683 Hodzic, A., Kasibhatla, P. S., Jo, D. S., Cappa, C. D., Jimenez, J. L., Madronich, S., and Park, R.
684   J.: Rethinking the global secondary organic aerosol (SOA) budget: stronger production,
685   faster removal, shorter lifetime, Atmos. Chem. Phys., 16, 7917-7941, 10.5194/acp-16-
686   7917-2016, 2016.
687 Holzinger, R., Kasper-Giebl, A., Staudinger, M., Schauer, G., and Rockmann, T.: Analysis of the
688   chemical composition of organic aerosol at the Mt. Sonnblick observatory using a novel
689   high mass resolution thermal-desorption proton-transfer-reaction mass-spectrometer (hr-
690   TD-PTR-MS), Atmospheric Chemistry and Physics, 10, 10111-10128, 10.5194/acp-10-
691   10111-2010, 2010.
692 Hu, W. W., Hu, M., Hu, W., Jimenez, J. L., Yuan, B., Chen, W. T., Wang, M., Wu, Y. S., Chen,
693   C., Wang, Z. B., Peng, J. F., Zeng, L. M., and Shao, M.: Chemical composition, sources,
694   and aging process of submicron aerosols in Beijing: Contrast between summer and
695   winter, Journal of Geophysical Research-Atmospheres, 121, 1955-1977,
696   10.1002/2015jd024020, 2016.
697 Huang, X. F., He, L. Y., Hu, M., Canagaratna, M. R., Sun, Y., Zhang, Q., Zhu, T., Xue, L., Zeng,
698   L. W., Liu, X. G., Zhang, Y. H., Jayne, J. T., Ng, N. L., and Worsnop, D. R.: Highly
699   time-resolved chemical characterization of atmospheric submicron particles during 2008
700   Beijing Olympic Games using an Aerodyne High-Resolution Aerosol Mass
701   Spectrometer, Atmospheric Chemistry and Physics, 10, 8933-8945, 10.5194/acp-10-
702   8933-2010, 2010.

703 Huang, X. F., He, L. Y., Hu, M., Canagaratna, M. R., Kroll, J. H., Ng, N. L., Zhang, Y. H., Lin,
704   Y., Xue, L., Sun, T. L., Liu, X. G., Shao, M., Jayne, J. T., and Worsnop, D. R.:
705   Characterization of submicron aerosols at a rural site in Pearl River Delta of China using
706   an Aerodyne High-Resolution Aerosol Mass Spectrometer, Atmospheric Chemistry and
707   Physics, 11, 1865-1877, 10.5194/acp-11-1865-2011, 2011.
708 Huang, X. F., Xue, L., Tian, X. D., Shao, W. W., Sun, T. L., Gong, Z. H., Ju, W. W., Jiang, B.,
709   Hu, M., and He, L. Y.: Highly time-resolved carbonaceous aerosol characterization in
710   Yangtze River Delta of China: Composition, mixing state and secondary formation,
711   Atmospheric Environment, 64, 200-207, 10.1016/j.atmosenv.2012.09.059, 2013.
712 Jathar, S. H., Farina, S. C., Robinson, A. L., and Adams, P. J.: The influence of semi-volatile and
713   reactive primary emissions on the abundance and properties of global organic aerosol,
714   Atmos. Chem. Phys., 11, 7727-7746, 2011.
715 Jo, D. S., Park, R. J., Kim, M. J., and Spracklen, D. V.: Effects of chemical aging on global
716   secondary organic aerosol using the volatility basis set approach, Atmos. Environ., 81,
717   230-244, 2013.
718 Jöckel, P., Tost, H., Pozzer, A., Bruehl, C., Buchholz, J., Ganzeveld, L., Hoor, P., Kerkweg, A.,
719   Lawrence, M. G., Sander, R., Steil, B., Stiller, G., Tanarhte, M., Taraborrelli, D., Van
720   Aardenne, J., and Lelieveld, J.: The atmospheric chemistry general circulation model
721   ECHAM5/MESSy1: consistent simulation of ozone from the surface to the mesosphere,
722   Atmos. Chem. Phys., 6, 5067-5104, 2006.
723 Karydis, V. A., Tsimpidi, A. P., Pozzer, A., Astitha, M., and Lelieveld, J.: Effects of mineral dust
724   on global atmospheric nitrate concentrations, Atmos. Chem. Phys., 16, 1491-1509,
725   10.5194/acp-16-1491-2016, 2016.
726 Karydis, V. A., Tsimpidi, A. P., Bacer, S., Pozzer, A., Nenes, A., and Lelieveld, J.: Global
727   impact of mineral dust on cloud droplet number concentration, Atmospheric Chemistry
728   and Physics, 17, 5601-5621, 10.5194/acp-17-5601-2017, 2017.
729 Kerkweg, A., Buchholz, J., Ganzeveld, L., Pozzer, A., Tost, H., and Jöckel, P.: Technical Note:
730   An implementation of the dry removal processes DRY DEPosition and SEDImentation in
731   the Modular Earth Submodel System (MESSy), Atmos. Chem. Phys., 6, 4617-4632,
732   2006a.
733 Kerkweg, A., Sander, R., Tost, H., and Jöckel, P.: Technical note: Implementation of prescribed
734   (OFFLEM), calculated (ONLEM), and pseudo-emissions (TNUDGE) of chemical
735   species in the Modular Earth Submodel System (MESSy), Atmos. Chem. Phys., 6, 3603-
736   3609, 10.5194/acp-6-3603-2006, 2006b.
737 Koo, B., Knipping, E., and Yarwood, G.: 1.5-Dimensional volatility basis set approach for
738   modeling organic aerosol in CAMx and CMAQ, Atmospheric Environment, 95, 158-164,
739   10.1016/j.atmosenv.2014.06.031, 2014.
740 Kuwata, M., and Lee, W. C.: 1-octanol-water partitioning as a classifier of water soluble organic
741   matters: Implication for solubility distribution, Aerosol Science and Technology, 51, 602-
742   613, 10.1080/02786826.2017.1283004, 2017.
743 Lambe, A. T., Onasch, T. B., Massoli, P., Croasdale, D. R., Wright, J. P., Ahern, A. T.,
744   Williams, L. R., Worsnop, D. R., Brune, W. H., and Davidovits, P.: Laboratory studies of
745   the chemical composition and cloud condensation nuclei (CCN) activity of secondary
746   organic aerosol (SOA) and oxidized primary organic aerosol (OPOA), Atmospheric
747   Chemistry and Physics, 11, 8913-8928, 10.5194/acp-11-8913-2011, 2011.

748 Lane, T. E., Donahue, N. M., and Pandis, S. N.: Simulating secondary organic aerosol formation
749 using the volatility basis-set approach in a chemical transport model, Atmos. Environ.,
750 42, 7439-7451, 2008.
751 Lauer, A., Eyring, V., Hendricks, J., Joeckel, P., and Lohmann, U.: Global model simulations of
752 the impact of ocean-going ships on aerosols, clouds, and the radiation budget, Atmos.
753 Chem. Phys., 7, 5061-5079, 2007.
754 Liggio, J., Li, S. M., Vlasenko, A., Sjostedt, S., Chang, R., Shantz, N., Abbatt, J., Slowik, J. G.,
755 Bottenheim, J. W., Brickell, P. C., Stroud, C., and Leaitch, W. R.: Primary and secondary
756 organic aerosols in urban air masses intercepted at a rural site, Journal of Geophysical
757 Research-Atmospheres, 115, 10.1029/2010jd014426, 2010.
758 Martin, S. T., Andreae, M. O., Althausen, D., Artaxo, P., Baars, H., Borrmann, S., Chen, Q.,
759 Farmer, D. K., Guenther, A., Gunthe, S. S., Jimenez, J. L., Karl, T., Longo, K., Manzi,
760 A., Muller, T., Pauliquevis, T., Petters, M. D., Prenni, A. J., Poschl, U., Rizzo, L. V.,
761 Schneider, J., Smith, J. N., Swietlicki, E., Tota, J., Wang, J., Wiedensohler, A., and Zorn,
762 S. R.: An overview of the Amazonian Aerosol Characterization Experiment 2008
763 (AMAZE-08), Atmospheric Chemistry and Physics, 10, 11415-11438, 10.5194/acp-10-
764 11415-2010, 2010.
765 Mohr, C., DeCarlo, P. F., Heringa, M. F., Chirico, R., Slowik, J. G., Richter, R., Reche, C.,
766 Alastuey, A., Querol, X., Seco, R., Penuelas, J., Jimenez, J. L., Crippa, M., Zimmermann,
767 R., Baltensperger, U., and Prevot, A. S. H.: Identification and quantification of organic
768 aerosol from cooking and other sources in Barcelona using aerosol mass spectrometer
769 data, Atmospheric Chemistry and Physics, 12, 1649-1665, 10.5194/acp-12-1649-2012,
770 2012.
771 Murphy, B. N., and Pandis, S. N.: Simulating the formation of semivolatile primary and
772 secondary organic aerosol in a regional chemical transport model, Environ. Sci. Technol.,
773 43, 4722-4728, 2009.
774 Murphy, B. N., Donahue, N. M., Fountoukis, C., and Pandis, S. N.: Simulating the oxygen
775 content of ambient organic aerosol with the 2D volatility basis set, Atmos. Chem. Phys.,
776 11, 7859-7873, 2011.
777 Murphy, B. N., Donahue, N. M., Fountoukis, C., Dall'Osto, M., O'Dowd, C., Kiendler-Scharr,
778 A., and Pandis, S. N.: Functionalization and fragmentation during ambient organic
779 aerosol aging: application of the 2-D volatility basis set to field studies, Atmospheric
780 Chemistry and Physics, 12, 10797-10816, 10.5194/acp-12-10797-2012, 2012.
781 Napier, W. J., Ensberg, J. J., and Seinfeld, J. H.: Insight into the numerical challenges of
782 implementing 2-dimensional SOA models in atmospheric chemical transport models,
783 Atmospheric Environment, 96, 331-344, 10.1016/j.atmosenv.2014.07.048, 2014.
784 Ng, N. L., Canagaratna, M. R., Zhang, Q., Jimenez, J. L., Tian, J., Ulbrich, I. M., Kroll, J. H.,
785 Docherty, K. S., Chhabra, P. S., Bahreini, R., Murphy, S. M., Seinfeld, J. H., Hildebrandt,
786 L., Donahue, N. M., DeCarlo, P. F., Lanz, V. A., Prévôt, A. S. H., Dinar, E., Rudich, Y.,
787 and Worsnop, D. R.: Organic aerosol components observed in Northern Hemispheric
788 datasets from Aerosol Mass Spectrometry, Atmos. Chem. Phys., 10, 4625-4641,
789 10.5194/acp-10-4625-2010, 2010.
790 Paciga, A., Karnezi, E., Kostenidou, E., Hildebrandt, L., Psichoudaki, M., Engelhart, G. J., Lee,
791 B. H., Crippa, M., Prevot, A. S. H., Baltensperger, U., and Pandis, S. N.: Volatility of
792 organic aerosol and its components in the megacity of Paris, Atmospheric Chemistry and
793 Physics, 16, 2013-2023, 10.5194/acp-16-2013-2016, 2016.

794 Pankow, J. F., and Asher, W. E.: SIMPOL.1: a simple group contribution method for predicting
795   vapor pressures and enthalpies of vaporization of multifunctional organic compounds,
796   Atmospheric Chemistry and Physics, 8, 2773-2796, 10.5194/acp-8-2773-2008, 2008.
797 Pozzer, A., Zimmermann, P., Doering, U. M., van Aardenne, J., Tost, H., Dentener, F., Janssens-
798   Maenhout, G., and Lelieveld, J.: Effects of business-as-usual anthropogenic emissions on
799   air quality, Atmos. Chem. Phys., 12, 6915-6937, 10.5194/acp-12-6915-2012, 2012.
800 Pringle, K. J., Tost, H., Message, S., Steil, B., Giannadaki, D., Nenes, A., Fountoukis, C., Stier,
801   P., Vignati, E., and Leieved, J.: Description and evaluation of GMXe: a new aerosol
802   submodel for global simulations (v1), Geoscientific Model Development, 3, 391-412,
803   2010.
804 Pye, H. O. T., and Seinfeld, J. H.: A global perspective on aerosol from low-volatility organic
805   compounds, Atmos. Chem. Phys., 10, 4377-4401, 2010.
806 Robinson, A. L., Donahue, N. M., Shrivastava, M. K., Weitkamp, E. A., Sage, A. M., Grieshop,
807   A. P., Lane, T. E., Pierce, J. R., and Pandis, S. N.: Rethinking organic aerosols:
808   Semivolatile emissions and photochemical aging, Science, 315, 1259-1262, 2007.
809 Roeckner, E., Brokopf, R., Esch, M., Giorgetta, M., Hagemann, S., Kornblueh, L., Manzini, E.,
810   Schlese, U., and Schulzweida, U.: Sensitivity of simulated climate to horizontal and
811   vertical resolution in the ECHAM5 atmosphere model, Journal of Climate, 19, 3771-
812   3791, 10.1175/jcli3824.1, 2006.
813 Saarikoski, S., Carbone, S., Decesari, S., Giulianelli, L., Angelini, F., Canagaratna, M., Ng, N.
814   L., Trimborn, A., Facchini, M. C., Fuzzi, S., Hillamo, R., and Worsnop, D.: Chemical
815   characterization of springtime submicrometer aerosol in Po Valley, Italy, Atmospheric
816   Chemistry and Physics, 12, 8401-8421, 10.5194/acp-12-8401-2012, 2012.
817 Sander, R., Baumgaertner, A., Gromov, S., Harder, H., Joeckel, P., Kerkweg, A., Kubistin, D.,
818   Regelin, E., Riede, H., Sandu, A., Taraborrelli, D., Tost, H., and Xie, Z. Q.: The
819   atmospheric chemistry box model CAABA/MECCA-3.0, Geoscientific Model
820   Development, 4, 373-380, 2011.
821 Shiraiwa, M., Berkemeier, T., Schilling-Fahnestock, K. A., Seinfeld, J. H., and Poschl, U.:
822   Molecular corridors and kinetic regimes in the multiphase chemical evolution of
823   secondary organic aerosol, Atmospheric Chemistry and Physics, 14, 8323-8341,
824   10.5194/acp-14-8323-2014, 2014.
825 Shiraiwa, M., Li, Y., Tsimpidi, A. P., Karydis, V. A., Berkemeier, T., Pandis, S. N., Lelieveld, J.,
826   Koop, T., and Poschl, U.: Global distribution of particle phase state in atmospheric
827   secondary organic aerosols, Nature Communications, 8, 10.1038/ncomms15002, 2017.
828 Sun, Y., Zhang, Q., Macdonald, A. M., Hayden, K., Li, S. M., Liggio, J., Liu, P. S. K., Anlauf,
829   K. G., Leaitch, W. R., Steffen, A., Cubison, M., Worsnop, D. R., van Donkelaar, A., and
830   Martin, R. V.: Size-resolved aerosol chemistry on Whistler Mountain, Canada with a
831   high-resolution aerosol mass spectrometer during INTEX-B, Atmospheric Chemistry and
832   Physics, 9, 3095-3111, 10.5194/acp-9-3095-2009, 2009.
833 Sun, Y. L., Zhang, Q., Schwab, J. J., Demerjian, K. L., Chen, W. N., Bae, M. S., Hung, H. M.,
834   Hogrefe, O., Frank, B., Rattigan, O. V., and Lin, Y. C.: Characterization of the sources
835   and processes of organic and inorganic aerosols in New York city with a high-resolution
836   time-of-flight aerosol mass apectrometer, Atmospheric Chemistry and Physics, 11, 1581-
837   1602, 10.5194/acp-11-1581-2011, 2011.
838 Timonen, H., Carbone, S., Aurela, M., Saarnio, K., Saarikoski, S., Ng, N. L., Canagaratna, M.
839   R., Kulmala, M., Kerminen, V. M., Worsnop, D. R., and Hillamo, R.: Characteristics,

840   sources and water-solubility of ambient submicron organic aerosol in springtime in
841   Helsinki, Finland, Journal of Aerosol Science, 56, 61-77, 10.1016/j.jaerosci.2012.06.005,
842   2013.
843 Tost, H., Jockel, P. J., Kerkweg, A., Sander, R., and Lelieveld, J.: Technical note: A new
844   comprehensive SCAVenging submodel for global atmospheric chemistry modelling,
845   Atmos. Chem. Phys., 6, 565-574, 2006.
846 Trail, M., Tsimpidi, A. P., Liu, P., Tsigaridis, K., Hu, Y., Nenes, A., and Russell, A. G.:
847   Downscaling a global climate model to simulate climate change over the US and the
848   implication on regional and urban air quality, Geoscientific Model Development, 6,
849   1429-1445, 10.5194/gmd-6-1429-2013, 2013.
850 Trail, M., Tsimpidi, A. P., Liu, P., Tsigaridis, K., Rudokas, J., Miller, P., Nenes, A., Hu, Y., and
851   Russell, A. G.: Sensitivity of air quality to potential future climate change and emissions
852   in the United States and major cities, Atmospheric Environment, 94, 552-563,
853   10.1016/j.atmosenv.2014.05.079, 2014.
854 Tsigaridis, K., Daskalakis, N., Kanakidou, M., Adams, P. J., Artaxo, P., Bahadur, R., Balkanski,
855   Y., Bauer, S. E., Bellouin, N., Benedetti, A., Bergman, T., Berntsen, T. K., Beukes, J. P.,
856   Bian, H., Carslaw, K. S., Chin, M., Curci, G., Diehl, T., Easter, R. C., Ghan, S. J., Gong,
857   S. L., Hodzic, A., Hoyle, C. R., Iversen, T., Jathar, S., Jimenez, J. L., Kaiser, J. W.,
858   Kirkevag, A., Koch, D., Kokkola, H., Lee, Y. H., Lin, G., Liu, X., Luo, G., Ma, X.,
859   Mann, G. W., Mihalopoulos, N., Morcrette, J. J., Mueller, J. F., Myhre, G.,
860   Myriokefalitakis, S., Ng, N. L., O'Donnell, D., Penner, J. E., Pozzoli, L., Pringle, K. J.,
861   Russell, L. M., Schulz, M., Sciare, J., Seland, O., Shindell, D. T., Sillman, S., Skeie, R.
862   B., Spracklen, D., Stavrakou, T., Steenrod, S. D., Takemura, T., Tiitta, P., Tilmes, S.,
863   Tost, H., van Noije, T., van Zyl, P. G., von Salzen, K., Yu, F., Wang, Z., Wang, Z.,
864   Zaveri, R. A., Zhang, H., Zhang, K., Zhang, Q., and Zhang, X.: The AeroCom evaluation
865   and intercomparison of organic aerosol in global models, Atmospheric Chemistry and
866   Physics, 14, 10845-10895, 10.5194/acp-14-10845-2014, 2014.
867 Tsimpidi, A. P., Karydis, V. A., Zavala, M., Lei, W., Molina, L., Ulbrich, I. M., Jimenez, J. L.,
868   and Pandis, S. N.: Evaluation of the volatility basis-set approach for the simulation of
869   organic aerosol formation in the Mexico City metropolitan area, Atmos. Chem. Phys., 10,
870   525-546, 2010.
871 Tsimpidi, A. P., Karydis, V. A., Zavala, M., Lei, W., Bei, N., Molina, L., and Pandis, S. N.:
872   Sources and production of organic aerosol in Mexico City: insights from the combination
873   of a chemical transport model (PMCAMx-2008) and measurements during MILAGRO,
874   Atmos. Chem. Phys., 11, 5153-5168, 2011.
875 Tsimpidi, A. P., Karydis, V. A., Pozzer, A., Pandis, S. N., and Lelieveld, J.: ORACLE (v1.0):
876   module to simulate the organic aerosol composition and evolution in the atmosphere,
877   Geoscientific Model Development, 7, 3153-3172, 10.5194/gmd-7-3153-2014, 2014.
878 Tsimpidi, A. P., Karydis, V. A., Pandis, S. N., and Lelieveld, J.: Global combustion sources of
879   organic aerosols: model comparison with 84 AMS factor-analysis data sets, Atmos.
880   Chem. Phys., 16, 8939-8962, 10.5194/acp-16-8939-2016, 2016.
881 Tsimpidi, A. P., Karydis, V. A., Pandis, S. N., and Lelieveld, J.: Global-scale combustion
882   sources of organic aerosols: sensitivity to formation and removal mechanisms,
883   Atmospheric Chemistry and Physics, 17, 7345-7364, 10.5194/acp-17-7345-2017, 2017.
884 Xu, L., Guo, H. Y., Boyd, C. M., Klein, M., Bougiatioti, A., Cerully, K. M., Hite, J. R.,
885   Isaacman-VanWertz, G., Kreisberg, N. M., Knote, C., Olson, K., Koss, A., Goldstein, A.

886 H., Hering, S. V., de Gouw, J., Baumann, K., Lee, S. H., Nenes, A., Weber, R. J., and Ng,
887 N. L.: Effects of anthropogenic emissions on aerosol formation from isoprene and
888 monoterpenes in the southeastern United States, Proceedings of the National Academy of
889 Sciences of the United States of America, 112, 37-42, 10.1073/pnas.1417609112, 2015.
890 Zhang, Q., Jimenez, J. L., Canagaratna, M. R., Allan, J. D., Coe, H., Ulbrich, I., Alfarra, M. R.,
891 Takami, A., Middlebrook, A. M., Sun, Y. L., Dzepina, K., Dunlea, E., Docherty, K.,
892 DeCarlo, P. F., Salcedo, D., Onasch, T., Jayne, J. T., Miyoshi, T., Shimono, A.,
893 Hatakeyama, S., Takegawa, N., Kondo, Y., Schneider, J., Drewnick, F., Borrmann, S.,
894 Weimer, S., Demerjian, K., Williams, P., Bower, K., Bahreini, R., Cottrell, L., Griffin, R.
895 J., Rautiainen, J., Sun, J. Y., Zhang, Y. M., and Worsnop, D. R.: Ubiquity and dominance
896 of oxygenated species in organic aerosols in anthropogenically-influenced Northern
897 Hemisphere midlatitudes, Geophys. Res. Lett., 34, doi: L13801 10.1029/2007gl029979,
898 2007.
899 Zhao, B., Wang, S. X., Donahue, N. M., Chuang, W. N., Hildebrandt Ruiz, L., Ng, N. L., Wang,
900 Y. J., and Hao, J. M.: Evaluation of One-Dimensional and Two-Dimensional Volatility
901 Basis Sets in Simulating the Aging of Secondary Organic Aerosol with Smog-Chamber
902 Experiments, Environmental Science & Technology, 49, 2245-2254, 10.1021/es5048914,
903 2015.

904
905

906

Table 1. Statistical evaluation of EMAC POA (sum of fPOA and bbPOA) against AMS POA

(sum of HOA and BBOA) from 61 data sets worldwide during 2001-2010.

909

Site Type	Number of datasets	Mean Observed ($\mu g\ m^{-3}$)	Mean Predicted ($\mu g\ m^{-3}$)	MAGE ($\mu g\ m^{-3}$)	MB ($\mu g\ m^{-3}$)	NME (%)	NMB (%)	RMSE ($\mu g\ m^{-3}$)
Urban Downwind	15	0.82	0.65	0.39	-0.17	47	-21	0.51
Rural/Remote	46	0.43	0.45	0.38	0.02	88	6	0.50
Season								
Winter	6	1.18	0.72	0.66	-0.45	56	-38	0.78
Spring	30	0.42	0.52	0.40	0.10	95	24	0.50
Summer	14	0.50	0.45	0.30	-0.05	60	-12	0.40
Autumn	11	0.49	0.41	0.28	-0.08	57	-18	0.38
Total	61	0.53	0.50	0.38	-0.03	72	-5	0.50

910

911

912

913   **Table 2.** Statistical evaluation of EMAC SOA against AMS OOA from 61 data sets worldwide

914   during 2001-2010.

915

Site Type	Number of datasets	Mean Observed ($\mu g\ m^{-3}$)	Mean Predicted ($\mu g\ m^{-3}$)	MAGE ($\mu g\ m^{-3}$)	MB ($\mu g\ m^{-3}$)	NME (%)	NMB (%)	RMSE ($\mu g\ m^{-3}$)
Urban Downwind	15	2.98	2.76	1.32	-0.22	44	-7	1.82
Rural/Remote	46	2.72	2.53	1.52	-0.18	56	-7	2.11
Season								
Winter	6	2.81	0.67	2.14	-2.14	76	-76	2.52
Spring	30	2.22	2.48	1.05	0.25	47	11	1.44
Summer	14	4.30	3.85	2.23	-0.45	52	-10	2.99
Autumn	11	2.35	2.34	1.29	-0.01	55	0	1.60
Total	61	2.78	2.59	1.47	-0.19	53	-7	2.04

916
917
918

919

920 **Table 3.** Statistical evaluation of EMAC aged SOA against AMS LVOOA from 41 data sets

921 worldwide during 2001-2010.

922

Site Type	Number of datasets	Mean Observed (µg m⁻³)	Mean Predicted (µg m⁻³)	MAGE (µg m⁻³)	MB (µg m⁻³)	NME (%)	NMB (%)	RMSE (µg m⁻³)
Urban Downwind	8	1.77	0.81	1.26	-0.95	71	-54	1.57
Rural/Remote	33	1.65	0.95	1.18	-0.70	72	-42	1.71
Season								
Winter	3	2.36	0.17	2.19	-2.19	93	-93	2.40
Spring	18	1.06	0.73	0.84	-0.33	79	-32	1.05
Summer	11	2.64	1.46	1.74	-1.18	66	-45	2.47
Autumn	9	1.49	0.92	0.92	-0.57	62	-38	1.14
Total	41	1.68	0.93	1.20	-0.75	72	-45	1.68

923

924
925
926   **Table 4.** Statistical evaluation of EMAC fresh SOA against AMS SVOOA from 41 data sets

927   worldwide during 2001-2010.

928

Site Type	Number of datasets	Mean Observed ($\mu g\ m^{-3}$)	Mean Predicted ($\mu g\ m^{-3}$)	MAGE ($\mu g\ m^{-3}$)	MB ($\mu g\ m^{-3}$)	NME (%)	NMB (%)	RMSE ($\mu g\ m^{-3}$)
Urban Downwind	8	0.81	1.22	0.75	0.41	92	50	0.98
Rural/Remote	33	1.03	1.35	0.82	0.32	79	31	1.03
Season								
Winter	3	0.87	0.36	0.51	-0.51	59	-59	0.63
Spring	18	0.54	0.88	0.66	0.34	122	64	0.91
Summer	11	1.89	2.22	1.08	0.33	57	17	1.19
Autumn	9	0.83	1.44	0.86	0.61	104	73	1.11
Total	41	0.99	1.32	0.80	0.33	81	34	1.02

929
930

931

932   **Table 5.** Worldwide O:C ratio predictions and observations of total OA.

Location	Lat	Lon	Time period	Measured O:C	Simulated O:C	Reference
Riverside, US	33.95	-117.4	14/07/05-13/08/05	0.35	0.57	Docherty et al. (2011)
Mexico City , MX	19.48	-99.15	10/03/06-30/03/06	0.41	0.55	Aiken et al. (2008)
Whistler, CA	50.01	-122.95	19/04/06-16/05/06	0.83	0.57	Sun et al. (2009)
Egbert, CA	44.23	-79.78	11/05/07-15/06/07	0.45	0.53	Liggio et al. (2010)
London, UK	51.53	-0.15	17/10/07-15/11/07	0.27	0.29	Allan et al. (2010)
Manaus, BR	-2.58	-60.2	07/02/08-14/03/08	0.44	0.50	Martin et al. (2010)
Po Valley, IT	44.65	11.62	30/03/08-20/04/08	0.47	0.56	Saarikoski et al. (2012)
Mace Head, IE	53.3	-9.8	16/05/08-13/06/08	0.53	0.65	Murphy et al. (2012)
Cabauw, NL	51.97	4.93	28/04/08-30/05/08	0.54	0.53	Murphy et al. (2012)
Beijing, CN	40.0	116.0	24/07/08-20/09/08	0.33	0.49	Huang et al. (2010)
West coast, CL	-20	-80	21/10/08-30/11/08	0.62	0.89	Hawkins et al. (2010)
Kaiping, CN	22.32	112.53	12/10/08-18/11/08	0.47	0.41	Huang et al. (2011)
Helsinki, FI	60.2	24.95	09/01/09-13/03/09	0.45	0.25	Carbone et al. (2014)
Barcelona, ES	41.39	2.12	25/02/09-26/03/09	0.36	0.50	Mohr et al. (2012)
Mace Head, IE	53.3	-9.8	26/02/09-26/03/09	0.58	0.65	Murphy et al. (2012)
Cabauw, NL	51.97	4.93	25/02/09-25/02/09	0.34	0.32	Murphy et al. (2012)
Helsinki, FI	60.2	24.95	09/04/09-08/05/09	0.51	0.46	Timonen et al. (2013)
Pasadena, US	34.14	-118.12	22/05/09-12/06/09	0.44	0.51	Guo et al. (2017)
Pasadena, US	34.14	-118.12	18/06/09-07/07/09	0.55	0.56	Guo et al. (2017)
New York, US	40.74	-73.92	13/07/09-03/08/09	0.36	0.55	Sun et al. (2011)
Pasadena, US	34.14	-118.12	10/07/09-04/08/09	0.48	0.55	Guo et al. (2017)
Paris, FR	48.83	2.36	01/07/09-31/07/09	0.38	0.54	Crippa et al. (2013)
Alps, AT	47.05	12.95	10/07/09-31/07/09	0.38	0.58	Holzinger et al. (2010)
Shenzhen, CN	22.6	113.9	25/10/09-02/12/09	0.30	0.41	He et al. (2011)
Fresno, US	36.81	-119.78	09/01/10-23/01/10	0.27	0.46	Ge et al. (2012)
Cool, US	38.88	-121.0	02/06/10-28/06/10	0.44	0.51	Xu et al. (2015)
Jiaxing, CN	30.8	120.8	29/06/10-15/07/10	0.28	0.42	Huang et al. (2013)
Guangzhou, CN	22.71	112.93	13/11/10-01/12/10	0.40	0.42	Gong et al. (2012)
Beijing, CN	40.0	116.0	22/11/10-22/12/10	0.32	0.20	Hu et al. (2016)
Jiaxing, CN	30.8	120.8	11/12/10-23/12/10	0.33	0.24	Huang et al. (2013)

933

934   **Table 6.** Worldwide O:C ratio predictions and observations of OOA.

Location	Lat	Lon	Time period	Measured O:C	Simulate O:C	Reference
Cheju Island, KR	33.51	126.50	11/04/01-30/04/01	0.84	0.64	Ng et al. (2010)
Manchester, UK	53.5	-2.22	14/06/01-25/06/01	0.81	0.72	Ng et al. (2010)
New York, US	40.74	-73.92	30/06/01-05/08/01	0.59	0.64	Ng et al. (2010)
Vancouver, CA	49.25	-123.13	11/08/01-24/08/01	0.56	0.59	Ng et al. (2010)
Manchester, UK	53.5	-2.22	17/01/02-28/01/02	0.47	0.61	Ng et al. (2010)
Hohenpeissenberg, DE	47.8	11.0	19/05/02-31/05/02	0.50	0.61	Ng et al. (2010)
East coast, US	37.95	-74.3	18/07/02-26/07/02	0.58	0.67	Ng et al. (2010)
Jungfraujoch, CH	46.3	7.6	28/06/02-17/07/02	0.70	0.63	Ng et al. (2010)
East coast, US	37.95	-74.3	29/07/02-10/08/02	0.60	0.70	Ng et al. (2010)
Pittsburgh, US	40.44	-79.94	06/09/02-22/09/02	0.51	0.60	Ng et al. (2010)
Fukue Island, JP	32.69	128.84	18/03/03-16/04/03	0.65	0.67	Ng et al. (2010)
Hyytiala, FI	61.8	24.3	31/03/05-15/04/05	0.47	0.64	Ng et al. (2010)
Boulder, US	40.02	-105.27	07/06/03-20/06/03	0.44	0.60	Ng et al. (2010)
Tokyo, JP	35.67	139.75	23/07/03-14/08/03	0.49	0.70	Ng et al. (2010)
NE London, UK	51.7	0.4	29/07/03-31/08/03	0.48	0.72	Ng et al. (2010)
Okinawa, JP	26.87	128.25	03/10/03-24/12/03	0.82	0.77	Ng et al. (2010)
Tokyo, JP	35.67	139.75	20/01/04-10/02/04	0.56	0.59	Ng et al. (2010)
New York, US	40.74	-73.92	07/01/04-06/02/04	0.45	0.58	Ng et al. (2010)
Norfolk coast, UK	53.0	1.1	25/04/04-26/05/04	0.70	0.69	Ng et al. (2010)
Wiesbaden, DE	50.22	8.45	14/07/04-04/08/04	0.57	0.63	Ng et al. (2010)
Pinnacle Park, US	43.0	-76	14/07/04-05/08/04	0.64	0.61	Ng et al. (2010)
Nova Scotia, CA	43.76	-66.1	07/07/04-14/08/04	0.65	0.68	Ng et al. (2010)
Mainz, DE	49.98	8.23	16/09/04-01/10/04	0.66	0.62	Ng et al. (2010)
Duke Forest, US	35.97	-79.1	13/09/04-21/09/04	0.46	0.60	Ng et al. (2010)
Roveredo, CH	46.23	9.12	01/03/05-15/03/15	0.43	0.58	Ng et al. (2010)
Harkingen, CH	47.32	7.82	12/05/05-30/05/15	0.55	0.63	Ng et al. (2010)
Riverside, US	33.95	-117.4	14/07/05-13/08/05	0.48	0.62	Ng et al. (2010)
Zurich, CH	47.4	8.5	14/07/05-04/08/05	0.51	0.65	Ng et al. (2010)
Thompson, US	43.11	-70.95	09/07/05-15/08/05	0.58	0.62	Ng et al. (2010)
Roveredo, CH	46.23	9.12	25/11/05-15/12/05	0.56	0.56	Ng et al. (2010)
Zurich, CH	47.4	8.5	06/01/06-25/01/06	0.65	0.54	Ng et al. (2010)
Reiden, CH	47.25	7.97	27/01/06-13/02/06	0.64	0.55	Ng et al. (2010)
Mexico City, MX	19.48	-99.15	10/03/06-30/03/06	0.53	0.69	Ng et al. (2010)
Payerne, CH	46.8	6.95	31/05/06-03/07/06	0.59	0.63	Ng et al. (2010)
Beijing, CN	40.0	116.0	09/07/06-21/07/06	0.50	0.65	Ng et al. (2010)
Massongex, CH	46.24	6.14	23/11/06-17/12/06	0.88	0.55	Ng et al. (2010)
Payerne, CH	46.8	6.95	12/01/07-17/02/07	0.50	0.61	Ng et al. (2010)
Rhine valley, CH	46.29	9	16/02/07-22/02/07	0.34	0.57	Ng et al. (2010)
Egbert, CA	44.23	-79.78	14/05/07-15/06/07	0.61	0.64	Ng et al. (2010)
Po Valley, IT	44.65	11.62	30/03/08-20/04/08	0.65	0.65	Saarikoski et al. (2012)
Finokalia, GR	35.33	25.66	08/05/08-04/06/08	0.80	0.73	Murphy et al. (2012)
Jungfraujoch, CH	46.3	7.6	01/05/08-29/05/08	0.70	0.65	Ng et al. (2010)
Beijing, CN	40.0	116.0	24/07/08-20/10/08	0.48	0.63	Huang et al. (2010)
Kaiping, CN	22.32	112.53	12/10/08-18/11/08	0.52	0.57	Huang et al. (2011)
Grenoble, FR	45.18	5.73	14/01/09-30/01/09	0.65	0.53	Ng et al. (2010)
Helsinki, FI	60.2	24.95	09/01/09-13/03/09	0.60	0.54	Carbone et al. (2014)
Barcelona, ES	41.39	2.12	25/02/09-26/03/09	0.58	0.61	Mohr et al. (2012)
Finokalia, GR	35.33	25.66	25/02/09-25/03/09	0.50	0.67	Murphy et al. (2012)
Helsinki, FI	60.2	24.95	09/04/09-08/05/09	0.58	0.63	Timonen et al. (2013)
New York, US	40.74	-73.92	13/07/09-03/08/09	0.50	0.64	Sun et al. (2011)
Shenzhen, CN	22.6	113.9	25/10/09-02/12/09	0.51	0.58	He et al. (2011)
Fresno, US	36.81	-119.78	09/01/10-23/01/10	0.42	0.62	Ge et al. (2012)
Pasadena, US	34.14	-118.12	15/05/10-16/06/10	0.58	0.61	Hayes et al. (2013)
Jiaxing, CN	30.8	120.8	29/06/10-15/07/10	0.41	0.60	Huang et al. (2013)
Guangzhou, CN	22.71	112.93	13/11/10-01/12/10	0.47	0.58	Gong et al. (2012)
Beijing, CN	40.0	116.0	22/11/10-22/12/10	0.53	0.57	Hu et al. (2016)
Jiaxing, CN	30.8	120.8	11/12/10-23/12/10	0.59	0.50	Huang et al. (2013)

938

939

940   **Table 7.** Statistical evaluation of EMAC O:C ratio of total OA against observations from 18 data

941   sets worldwide during 2001-2010.

Season	Number of datasets	Mean Observed ($\mu g\ m^{-3}$)	Mean Predicted ($\mu g\ m^{-3}$)	MAGE ($\mu g\ m^{-3}$)	MB ($\mu g\ m^{-3}$)	NME (%)	NMB (%)	RMSE ($\mu g\ m^{-3}$)
Winter	4	0.42	0.35	0.10	-0.07	24	-17	0.12
Spring	8	0.53	0.53	0.09	0.00	16	1	0.11
Summer	4	0.37	0.51	0.14	0.14	38	38	0.15
Autumn	2	0.51	0.65	0.14	0.14	28	28	0.19
Total	18	0.47	0.50	0.11	0.03	23	7	0.13

942

943

944   **Table 8.** Statistical evaluation of EMAC O:C ratio of OOA against observations from 18 data

945   sets worldwide during 2001-2010.

Season	Number of datasets	Mean Observed ($\mu g\ m^{-3}$)	Mean Predicted ($\mu g\ m^{-3}$)	MAGE ($\mu g\ m^{-3}$)	MB ($\mu g\ m^{-3}$)	NME (%)	NMB (%)	RMSE ($\mu g\ m^{-3}$)
Winter	7	0.58	0.56	0.14	-0.02	23	-4	0.17
Spring	12	0.63	0.65	0.08	0.02	13	4	0.10
Summer	10	0.58	0.65	0.09	0.07	15	12	0.11
Autumn	3	0.58	0.65	0.10	0.07	17	11	0.10
Total	32	0.60	0.63	0.10	0.03	16	5	0.12
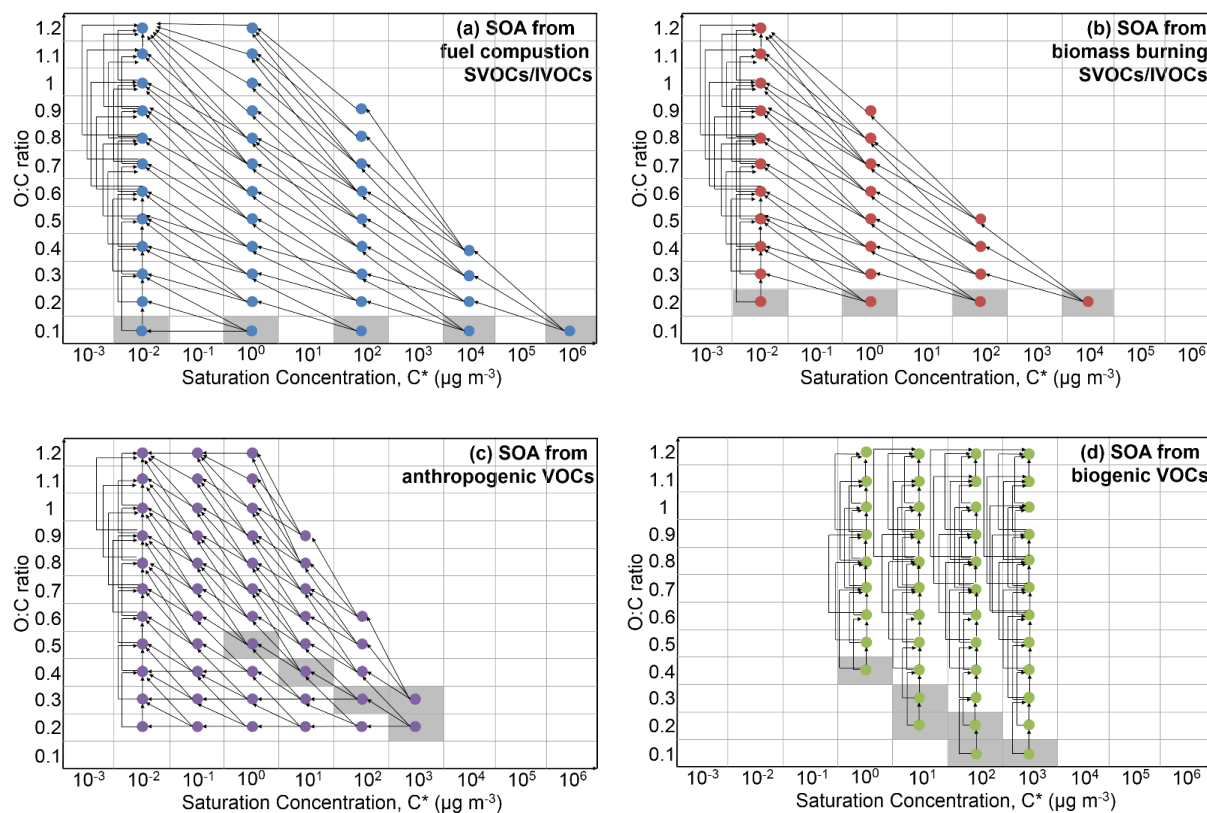
Figure 1: The 2-D grid space in ORACLE 2-D module with saturation concentration (in µg m^{-3}) on the x-axis and the O:C ratio on the y-axis. For each cell an organic surrogate compound is defined with a specific carbon number calculated as a function of effective saturation concentration and O:C ratio. The formation and evolution of SOA from: **(a)** fuel combustion SVOCs and IVOCs, **(b)** biomass burning SVOCs and IVOCs, **(c)** anthropogenic VOCs and, **(d)** biogenic VOCs are shown. The arrows correspond to the aging reactions and the grey grids to the initial chemical state of the species prior to aging.
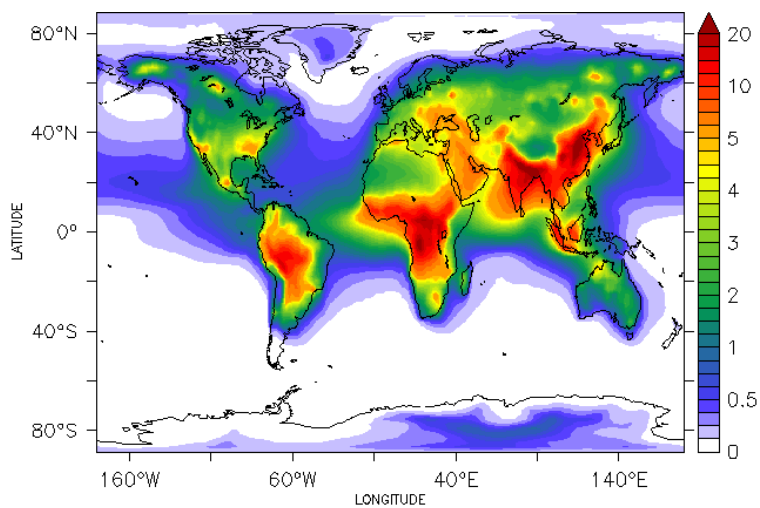
Figure 2: Predicted average surface concentration of total OA ($\mu g\ m^{-3}$) during the years 2001-2010.

960
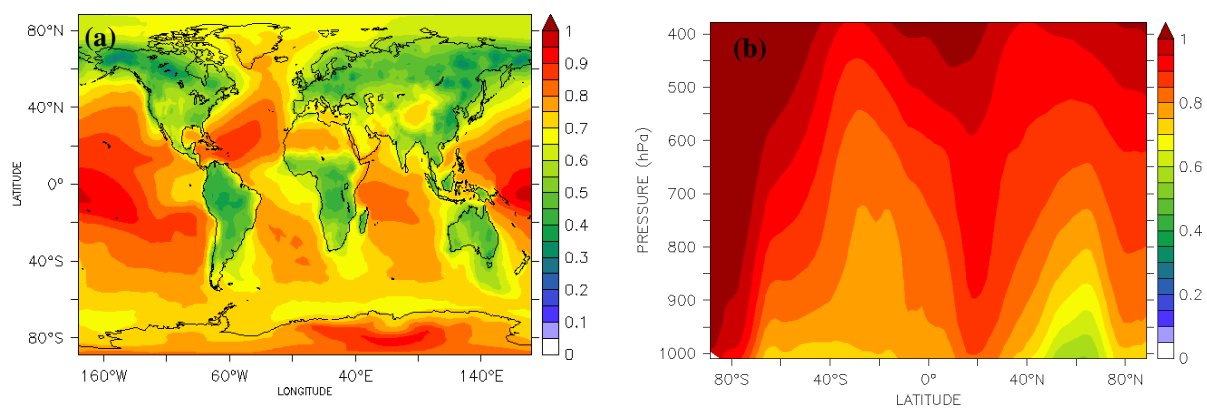
Figure 3: Predicted **(a)** average surface and **(b)** average zonal concentrations of total O:C during the years 2001-2010.
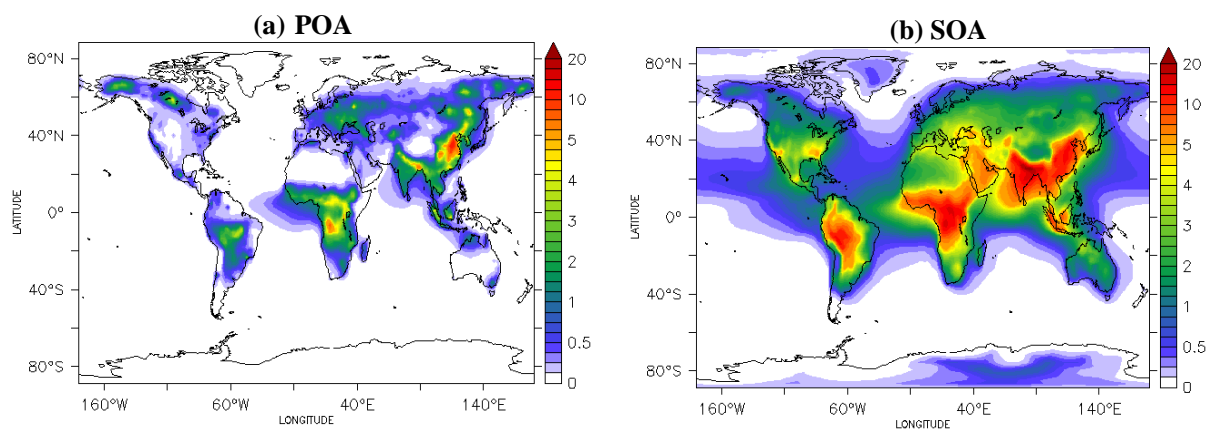
Figure 4: Predicted average surface concentration of **(a)** POA (μg m^{-3}) and **(b)** SOA (μg m^{-3})
during the years 2001-2010.

965
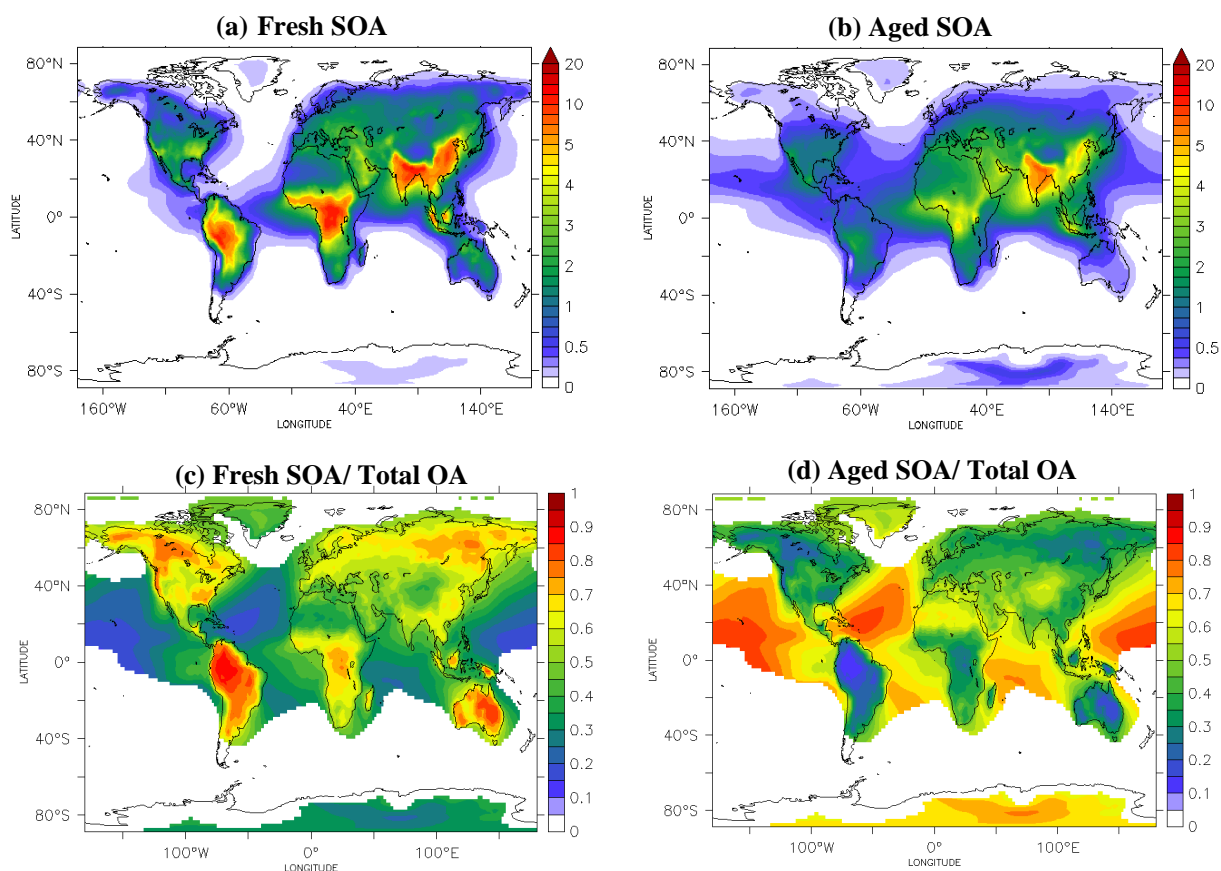
Figure 5: Predicted average surface concentration (in μg m^{-3}) of **(a)** fresh SOA and **(b)** aged

SOA and surface fraction of **(c)** fresh SOA and **(d)** aged SOA to total OA during the years 2001-
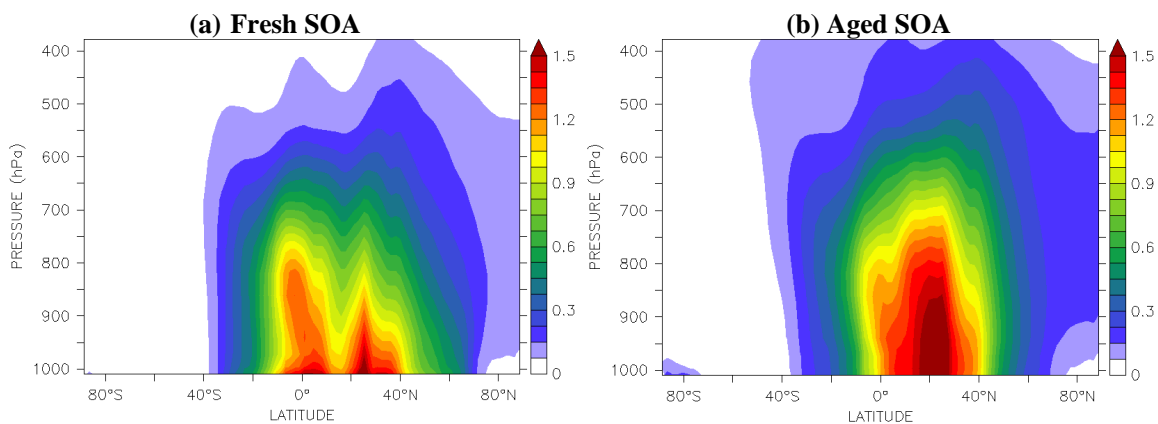
2010.

Figure 6: Predicted average zonal concentration (in μg m⁻³) of **(a)** fresh SOA and **(b)** aged SOA during the years 2001-2010.
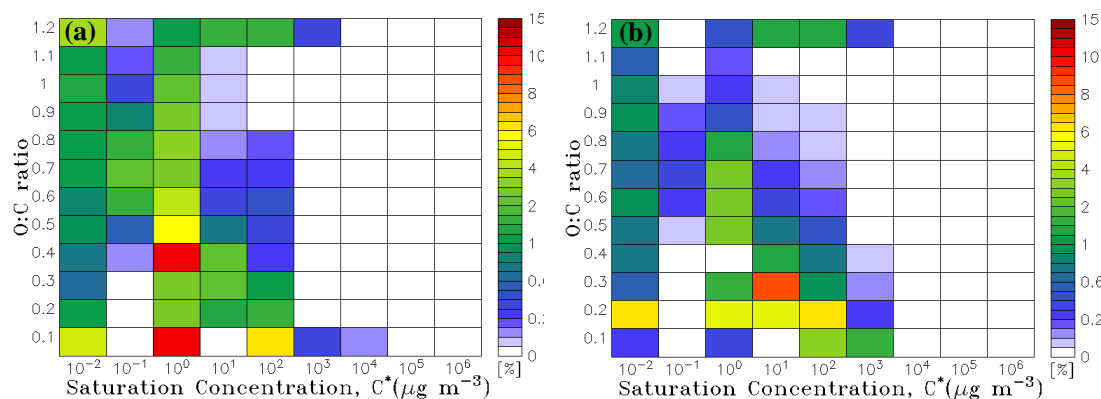
Figure 7: The average predicted fraction of OA concentration in each cell of the ORACLE 2-D
grid space to total OA concentration over **(a)** Europe and **(b)** the Amazon basin during the years
2001-2010.

974
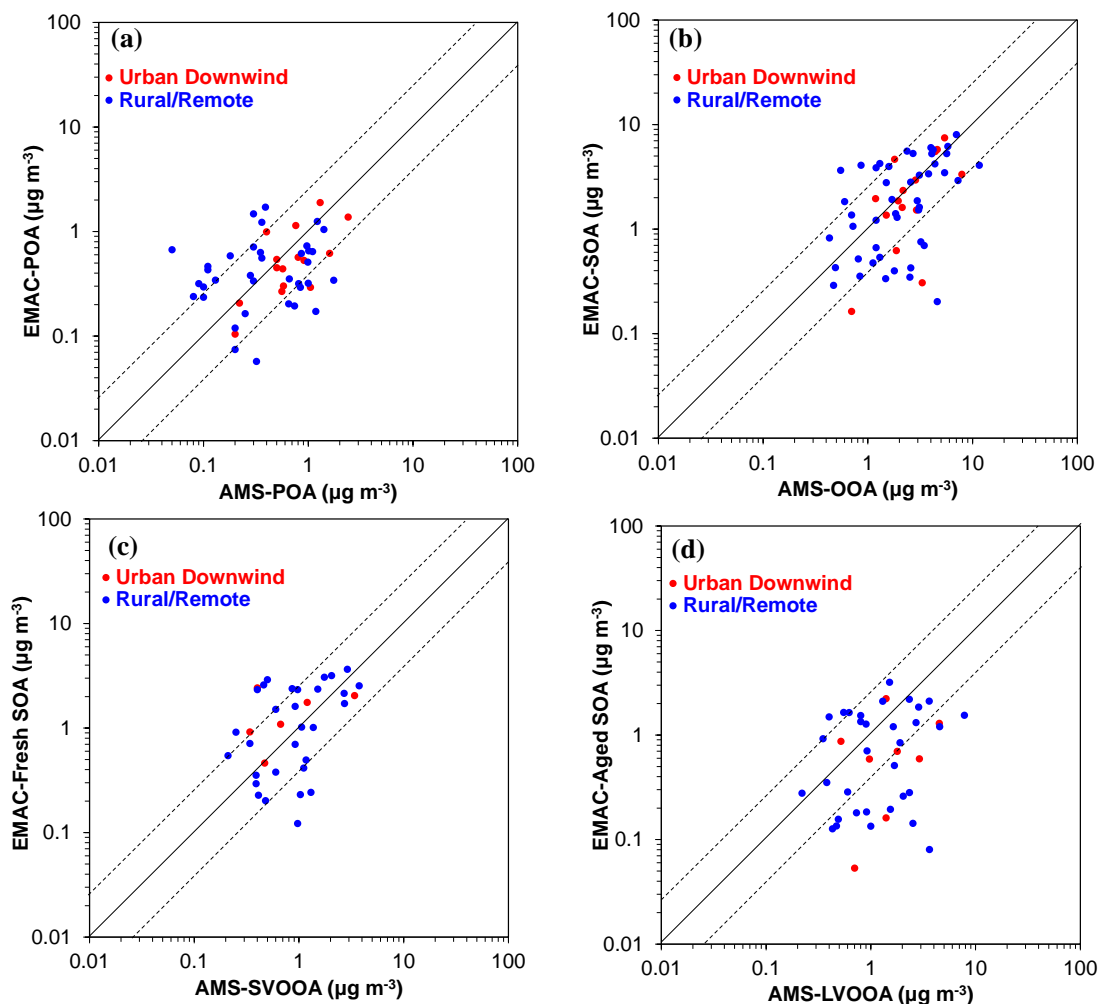
Figure 8: Scatterplots comparing model predictions to AMS measurements and their PMF analysis for: **(a)** POA, **(b)** OOA, **(c)** SV-OOA, and **(d)** LV-OOA concentrations (in μg m^{-3}) in the Northern Hemisphere during 2001-2010. Each point represents the data set average value over urban downwind (in red) and rural/remote (in blue) sites. Also shown are the 1:1, 2:1, and 1:2 lines.

980
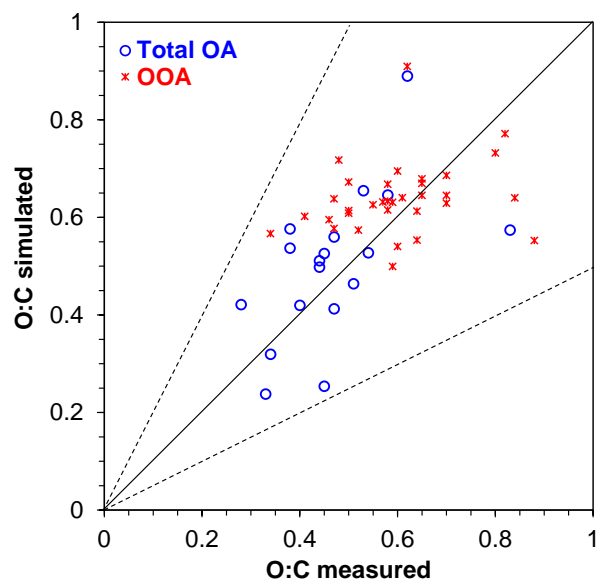
Figure 9: Scatterplot comparing model predictions to measurements for O:C ratio of total OA (in blue) and OOA (in red) over non-urban areas in the Northern Hemisphere during 2001-2010. Each point represents the data set average value over a specific measurement site. Also shown are the 1:1, 2:1, and 1:2 lines.